

Bayesian Inference with the l_1 -ball Prior: Solving Combinatorial Problems with Exact Zeros

Maoran Xu

Department of Statistical Science, Duke University, Durham, USA

Leo L. Duan

Department of Statistics, University of Florida, Gainesville, USA

February 22, 2023

Abstract

The l_1 -regularization is very popular in high dimensional statistics — it changes a combinatorial problem of choosing which subset of the parameter is zero, into a simple continuous optimization. Using a continuous prior concentrated near zero, the Bayesian counterparts are successful in quantifying the uncertainty in the variable selection problems; nevertheless, the lack of exact zeros makes it difficult for broader problems such as change-point detection and rank selection. Inspired by the duality of the l_1 -regularization as a constraint onto an l_1 -ball, we propose a new prior by projecting a continuous distribution onto the l_1 -ball. This creates a positive probability on the ball boundary, which contains both continuous elements and exact zeros. Unlike the spike-and-slab prior, this l_1 -ball projection is continuous and differentiable almost surely, making the posterior estimation amenable to the Hamiltonian Monte Carlo algorithm. We examine the properties, such as the volume change due to the projection, the connection to the combinatorial prior, the minimax concentration rate in the linear problem. We demonstrate the usefulness of exact zeros that simplify the combinatorial problems, such as the change-point detection in time series, the dimension selection of mixture models, and the low-rank-plus-sparse change detection in medical images.

Keywords:: Cardinality, Data Augmentation, Reversified Projection, Soft-Thresholding.

1 Introduction

The l_1 -regularization has been a milestone in high dimensional statistics. Since its introduction in the lasso regression for solving the variable selection problem (Tibshirani, 1996), it has inspired a rich class of algorithms and models — an incomplete list of representative works cover areas of regression (Efron et al., 2004; Zou and Hastie, 2005; Yuan and Lin, 2006), multivariate data analysis (Chen et al., 2001; Zou et al., 2006), graph estimation (Shojaie and Michailidis, 2010; Zhang and Zou, 2014; Fan et al., 2017), among others. For comprehensive reviews, see Meinshausen and Bühlmann (2006), and more recently Bühlmann and Van De Geer (2011).

One of the most appealing properties of l_1 -regularization is that it induces exact zeros in the optimal solution, hence bypassing the need to decide which subset of the parameter should be zero. This is due to the well-known dual form of the l_1 -norm penalty, as equivalent to constraining the parameter on an l_1 -ball centered at the origin. The “spikiness” of the l_1 -ball in high dimension makes it possible for a sparse recovery of the signals [See Vershynin (2018) for a formal exposition].

In recent years, it has been demonstrated that the sparse property can be exploited beyond the simple tasks of variable selection. In particular, some complicated combinatorial problems can be solved (or relaxed) via an “*over-parameterize and then sparsify*” strategy, using the l_1 -regularization. To give a few concrete examples, in the change-point detection of time series data, the fused lasso (Tibshirani et al., 2005) over-parameterizes each time point with an individual mean, then induces sparsity in the temporal increments/decrements; effectively, this leads to a step function that captures any abrupt temporal changes. For clustering problems, the sum-of-norms clustering (Lindsten et al., 2011; Tan and Witten, 2015) assigns a location parameter to every data point, then sparsifies the pairwise distance matrix; this induces only a few unique locations as the cluster centers. In the low-rank matrix smoothing/imputation, one uses an unconstrained matrix as the smoothed mean, then adds the nuclear norm regularization (Grave et al., 2011) as equivalent to sparsifying the singular values; this effectively achieves a rank selection on the matrix. These are just a few examples; nevertheless, it is not hard to see the equivalent combinatorial problems would be quite difficult to handle directly.

Most of the above models have been developed with an optimization focus; in parallel, the Bayesian literature is expanding rapidly to address the uncertainty quantification problems, in particular: (i) how likely a parameter element is zero or non-zero? (ii) how much correlation there is between the non-zero elements? These questions are important for the downstream statistical inference, such as building credible intervals and testing hypotheses. Among the early work, the Bayesian lasso exponentiates the negative l_1 -norm in a double exponential prior (Park and Casella, 2008); however, it was discovered that except for the posterior mode, the posterior of the Bayesian lasso has very little concentration near zero, while the thin tails cause an under-estimation of the non-zero signal. To address these issues, a rich class of continuous shrinkage priors has been proposed, with a large concentration in a neighborhood near zero and a heavy tail to accommodate large signals. Examples include the horseshoe (Carvalho et al., 2010), generalized double Pareto (Armagan et al., 2013), Dirichlet-Laplace (Bhattacharya et al., 2015), Beta-prime (Bai and Ghosh, 2019), spike-and-slab lasso (Ročková and George, 2018); among others. Due to the use of continuous priors, the posterior computation can be carried out efficiently using the Markov chain Monte Carlo methods (Bhattacharya et al., 2016); this is advantageous compared to the classic spike-and-slab prior, which involves a combinatorial prior that selects a subset of parameters to be non-zero (Mitchell and Beauchamp, 1988).

In these Bayesian models, although the posterior is not exactly zero, the close-to-zero estimates are adequate for the common variable selection problems. However, for the above over-parameterize-then-sparsify strategy, it faces challenges to build the Bayesian equivalency using the continuous shrinkage priors. First, the success of such a strategy would require some *transform* of the parameter to be zero (for example, the sum of changes over a long period of time in the change-point detection case). To that end, the continuous shrinkage prior placed on the individual elements, collectively, does not have a sufficiently large probability for the transform to be near zero. Second, there are problems in assigning a prior directly on the transform. Most importantly, the transform is often in a constrained space (for example, the distance matrix for points in \mathbb{R}^p being low-rank); hence the prescribed prior density is in fact incomplete, missing an intractable normalizing that could have an impact on the amount of shrinkage.

To address this issue, as well as to encourage developing novel combinatorial models, we propose a new strategy: starting from a continuous random variable with unconstrained support, we project it onto the l_1 -ball. This induces a distribution allowing the random variable to contain exact zeros. Since the projection is a continuous and differentiable transformation almost surely, we can use the popular off-the-shelf sampling algorithms such as the Hamiltonian Monte Carlo for the posterior computation. We are certainly not the first to consider a projection/transformation-approach for Bayesian modeling. For example, Gunn and Dunson (2005) used it for handling

monotone and unimodal constraints, Lin and Dunson (2014) for inducing monotone Gaussian process, Jauch et al. (2020) for satisfying orthonormal matrix constraint, and most recently, Sen et al. (2018) for a theoretic study on the projection of the posterior. Although we are inspired by those methods, our focus is not to satisfy the parameter constraints, but to use the *boundary* of a constrained set to induce a low-dimensional measure — in this case, any point outside the l_1 -ball will be projected onto the boundary, we obtain a positive probability for the random variable (or its transform) to contain both continuous elements and exact zeros. To our best knowledge, this idea is new.

We will illustrate the details of the projection, and its properties such as the volume change due to the projection, the connection to the combinatorial prior, and the minimax concentration rate in the linear problem. In the applications, we will demonstrate the usefulness of exact sparsity in a few Bayesian models of combinatorial problems, such as piece-wise constant smoothing, dimension selection in the finite mixture model, and the low-rank matrix smoothing with an application in medical image analysis.

2 The l_1 -ball Prior

In this section, we propose a new prior construction of producing exact sparsity in a probabilistic framework. We start from several motivating examples, and then introduce the prior while addressing three questions : (i) how to use an l_1 -ball projection to change a continuous random variable into a mixed-type random variable, which contains both continuous elements and zeros? (ii) how to calculate the associated probability after the projection? (iii) how to assign prior on the radius of an l_1 -ball?

2.1 Motivating Combinatorial Problems

To motivate a new class of priors on the l_1 -ball, we first list a few interesting combinatorial problems that can be significantly simplified using our approach. We will use $\theta \in \mathbb{R}^p$ to denote the parameter of interest.

(a) Sparse contrast models. Often in time series and image data applications, we want to estimate some underlying group structure, with each group defined as a continuous or uninterrupted temporal period or spatial region. Those models can often be re-parameterized as having sparse contrast $D\theta$, with a contrast matrix $D \in \mathbb{R}^{d \times p}$ (each row of D adding to zero). For example, in image smoothing/boundary detection, one could use sparse $(\theta_i - \theta_j)$'s between all neighboring pixels to induce a piece-wise constant structure in the mean. This idea has led to the success of fused lasso approaches using l_1 -norm on $D\theta$ for obtaining point estimates in optimization (Tibshirani and Taylor, 2011). On the other hand, because there are more contrasts than pixels in an image ($d \approx 2p$ in a two-dimensional image), the sparse set $\{x \in \mathbb{R}^d : x = D\theta\}$ is the column space of D with intrinsic dimension at most p , hence is challenging to directly assign a sparse prior via conventional Bayesian approaches.

(b) Reduced dimension models. It is common in Bayesian models to consider θ as a high-dimensional parameter residing near a low-dimensional space so that it can achieve approximate dimension reduction. However, there are cases when it is preferable to induce an exactly low dimension instead of approximation. For example, in clustering data analysis using mixture models, often we want to estimate the number of clusters; and it has been shown that having a low-dimensional mixture weight can lead to a consistent estimate on the number of clusters (Miller and Harrison, 2018), whereas continuous shrinkage priors (such as Dirichlet process prior) can result in an overestimation. As another example, to parameterize a block-diagonal matrix θ (subject to row and column permutation), often used for community detection in network data

analysis, one could control its Laplacian matrix L_θ to be exactly low-rank Anderson Jr and Morley (1985).

(c) Structured/dependent sparsity models. There has already been rich literature on using sparsity models for variable selection in regression; nevertheless, there is a growing interest in inducing correlation/dependent structure within the parameter (Hoff, 2017; Griffin and Hoff, 2019). For example, there may be prior knowledge that some elements in θ are more likely to be simultaneously zero.

Although there are some methods developed specifically for each scenario listed above, we will show that our new prior provides a simple solution that enables an arguably more straightforward prior specification and tractable posterior estimation. Our proposal can be summarized as the following prior generating process:

$$\begin{aligned}\beta &\sim \pi_\beta, \quad r \sim \pi_r, \\ \theta &= P_{\mathbb{B}_{h,r}}(\beta),\end{aligned}\tag{1}$$

where $\beta \in \mathbb{R}^p$ is a continuous random variable from distribution π_β (we slightly abuse notations by letting π_β denote both distribution and associated density function), and $r > 0$ is a scalar-valued random variable that we refer to as the radius and is from distribution π_r , $\mathbb{B}_{h,r} = \{x : \|h(x)\|_1 \leq r\}$ is an l_1 -ball associated with a function $h : \mathbb{R}^p \rightarrow \mathbb{R}^d$, and $P_{\mathbb{B}_{h,r}}(\cdot)$ denotes a projection equal to $\operatorname{argmin}_x \|x - \beta\|_2^2$ with $x \in \mathbb{B}_{h,r}$. Later, we will show how to build models for cases (a) and (b) with some suitable choices of h , and how to induce dependence structure in θ for case (c) by adopting a correlated distribution for π_β .

It is not hard to see that (1) gives a joint prior distribution $\pi_{\theta,r}(\theta, r) = \pi_r(r)\pi_{\theta|r}(\theta)$, we will describe $\pi_{\theta|r}$ in Sections 2.2 and 2.3, and π_r in Section 2.4. For now, for better clarity, we first focus on the identity function $h(x) = x$, show how an l_1 -ball projection leads to sparsity, and characterize the probabilities associated with (1).

Remark 1. *To clarify, our approach is equivalent to reparameterizing a sparse θ [or θ with sparse $h(\theta)$] using continuous β . In a diagram, our modeling framework is*

$$\theta \sim \pi(\theta | y) = \frac{\mathcal{L}(y; \theta)\pi_\theta(\theta)}{\int \mathcal{L}(y; \theta)\pi_\theta(\theta)d\theta}, \quad \text{with } \theta = P_{\mathbb{B}}(\beta).$$

As β effectively enters the likelihood $\mathcal{L}(y; \theta)$ and posterior $\pi(\theta | y)$, this is a fully Bayesian model that gives uncertainty quantification and enables inferences on sparsity. Further, this reparameterization does not depend on the form of likelihood, hence our method does not require the posterior to be log-concave.

To compare, there have been several post-processing approaches based on first sampling θ from a continuous posterior, then producing sparse θ^* via some transform (Bondell and Reich, 2012; Hahn and Carvalho, 2015; Li and Pati, 2017). In a diagram, they can be understood as two-stage estimators:

$$(i) \theta \sim \pi(\theta | y) = \frac{\mathcal{L}(y; \theta)\pi_\theta(\theta)}{\int \mathcal{L}(y; \theta)\pi_\theta(\theta)d\theta}. \quad (ii) \theta^* = T(\theta),$$

for some post-processing mapping T . Note that the sparse θ^* does not influence the likelihood, and corresponds to zero posterior probability (due to θ being continuous posterior). As a result, these approaches cannot be used for inference tasks such as estimating the $(1 - \tilde{\alpha})$ -credit interval on $\|\theta\|_0$ (number of non-zeros) and $(1 - \tilde{\alpha})$ -prediction interval for $x^{*\top}\theta$ for a new x^* . We provide a detailed comparison in the supplementary materials.

2.2 Creating Sparse Prior via an l_1 -ball Projection

To ease notation, we now use $\mathbb{B}_r = \{x \in \mathbb{R}^p : \|x\|_1 \leq r\}$ as a shorthand for the vector-norm l_1 -ball $\mathbb{B}_{h,r}$ with $h(x) = x$. We denote the interior set by $\mathbf{int} \mathbb{B}_r = \{x \in \mathbb{R}^p : \|x\|_1 < r\}$, and boundary set by $\mathbf{bd} \mathbb{B}_r = \{x : \|x\|_1 = r\}$. For any point $\beta \in \mathbb{R}^p$, we can project it onto the l_1 -ball, by solving the following problem,

$$\theta = P_{\mathbb{B}_r}(\beta) = \arg \min_{\|x\|_1 \leq r} \|\beta - x\|_2^2.$$

The loss function on the right hand side is strictly convex — that is, for every β , there is only one optimal solution $\theta = P_{\mathbb{B}_r}(\beta)$ (the mapping is measurable). For the sake of completeness, we present a simple algorithm [modifying from Duchi et al. (2008)]: if $\|\beta\|_1 \leq r$, let $\theta = \beta$; If $\|\beta\|_1 > r$,

$$\begin{aligned} & \text{sort } \beta \text{ so that } |\beta_{(1)}| \geq \dots \geq |\beta_{(p)}|, \\ & c := \max \left\{ j : |\beta_{(j)}| > \frac{\mu_j}{j}, \mu_j = \left(\sum_{i=1}^j |\beta_{(i)}| - r \right)_+ \right\}, \\ & \theta_i := \text{sign}(\beta_i) \left(|\beta_i| - \frac{\mu_c}{c} \right)_+, \end{aligned} \tag{2}$$

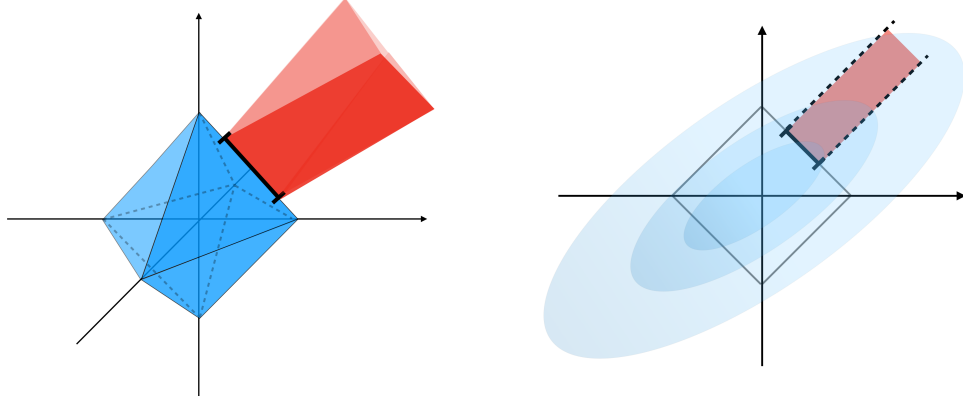
where $(x)_+ = \max\{x, 0\}$.

We now examine the induced probability distribution of θ . Suppose $\beta \in \mathbb{R}^p$ is a continuous random variable, in a probability space $(\mathbb{R}^p, \mathcal{B}(\mathbb{R}^p), \nu)$, with ν its measure absolutely continuous with respect to the Lebesgue measure in \mathbb{R}^p , and π_β the associated density. We can compute the probability for θ in any set \mathcal{A} in \mathbb{B}_r :

$$\text{pr}(\theta \in \mathcal{A}) = \int_{\mathbb{R}^p} \mathbb{I}[P_{\mathbb{B}_r}(x) \in \mathcal{A}] \pi_\beta(x) dx, \tag{3}$$

where $\mathbb{I}(E) = 1$ if the event E is true, otherwise takes value 0. Combining (2) and (3), we see two interesting results when we project from the outside $\beta : \|\beta\|_1 > r$:

1. It yields θ with $\|\theta\|_1 = r$, hence we have θ in the boundary set. Since all the points outside the ball will be projected to $\theta \in \mathbf{bd} \mathbb{B}_r$, the boundary set has a positive probability.
2. If the projection has $c < p$, there will be $(p - c)$ elements with $\theta_i = 0$.



(a) All the points β in the red area are projected to θ in the line segment $\{(x, 0, r - x) : 0.2 < x < 0.8\}$, which contains exact zero $\theta_2 = 0$.

(b) Sectional view in 2-dimensions: the probability of θ in the line segment is equal to the measure of β over the area in the red, which is positive.

Figure 1: Projecting a continuous Gaussian $\beta \in \mathbb{R}^3$ to θ onto an l_1 -ball \mathbb{B}_r (the right panel shows a density contour in 2-dimensions): the boundary set of θ containing exactly zero has a positive probability. For example, the probability of θ in the line segment $\{(x, 0, r - x) : 0.2 < x < 0.8\}$ is equal to the probability of β over the red region.

With those two properties, we see that θ will be sparse with a prior probability greater than zero, at a given r . Further, we now consider r as another random variable.

Note that the projection (2) is equivalent to finding a threshold $\tilde{\mu}$ to make the smallest few elements $|\beta_{(i)}| \leq \tilde{\mu}$ zero, and having the rest shrink by $\tilde{\mu}$ and $\sum_{i=1}^c [|\beta_{(i)}| - \tilde{\mu}] = r$. Therefore, using the joint prior of $(\beta_1, \dots, \beta_p, r)$, we can find a lower bound probability of obtaining at least k zeros after projection:

$$\begin{aligned} \text{pr}(\theta \text{ has at least } k \text{ zeros}) &\geq \text{pr}\left[\sum_{i=1}^{p-k} |\beta_{(i)}| \geq r + (p-k)|\beta_{(p-k+1)}|\right], \\ &= \text{pr}\left\{r \leq \sum_{i=1}^{p-k} [|\beta_{(i)}| - |\beta_{(p-k+1)}|]\right\} \end{aligned}$$

where the first line on the right corresponds to a sufficient condition for inducing exactly k zeros: to have $\sum_{i=1}^{p-k} [|\beta_{(i)}| - \tilde{\mu}] = r$, we need $\tilde{\mu} \geq |\beta_{(p-k+1)}|$, this makes all $(\beta_{(j)} - \tilde{\mu})_+ = 0$ for $j = p - k + 1, \dots, p$. Since $|\beta_{(i)}| - |\beta_{(p-k+1)}| > 0$ almost surely, with a suitable prior π_r for r , the above probability is strictly positive for any choice of $k = 1, \dots, (p-1)$.

To illustrate the geometric intuition, we show the projection in \mathbb{R}^3 (Figure 1) — projecting β from a multivariate Gaussian to $\theta \in \mathbb{B}_r$ gives us positive probability $\text{pr}[\theta = (x_1, 0, x_3)] > 0$, which equals to the Gaussian measure in the wedge region outside \mathbb{B}_r . Note that this is quite different from the conventional setting where θ is assigned a continuous prior in \mathbb{R}^p , for which fixing any $\theta_i = 0$ would cause the probability to collapse to zero.

From now on, we refer to the prior π_θ induced by a projection $P_{\mathbb{B}_r}$ to the vector-norm l_1 -ball defined via $\|\theta\|_1$ as an “ l_1 -ball prior”. For the more general case using a projection $P_{\mathbb{B}_{h,r}}$ to the l_1 -ball defined via $\|h(\theta)\|_1$, we refer to it as a “generalized l_1 -ball prior” and will defer its discussion to Section 2.4.

2.3 Closed-form Kernel for the Vector-norm l_1 -ball Prior

We now show that the prior of θ induced by $P_{\mathbb{B}_r}$ has a closed-form kernel (the combination of probability mass and density functions), and we denote it by $\pi_{\theta|r} : \mathbb{B}_r \rightarrow [0, \infty)$. For now, we treat r as given and will discuss its prior π_r in the next subsection.

To introduce some notations, we let $[p] = \{1, \dots, p\}$ be the full element indices, and $C = \{i \in [p] : \theta_i \neq 0\}$ a subset for those non-zero elements with $c := |C|$. And we use subscript to denote the non-zero sub-vector $\theta_C = (\theta_i)_{i \in C}$.

We now divide the l_1 -ball projection into two steps: (i) one-to-one transform of β into a set of latent variables; (ii) integrating over those falling below zero, as equivalent to the zero-thresholding in (2).

Step (i) produces the following latent variables:

$$t_i := |\beta_i| - \frac{\mu}{c}, \quad s_i := \text{sign}(\beta_i) \quad \text{for } i \in [p],$$

$$\mu := \mu_c, \quad c = \max\{j : |\beta_{(j)}| > \frac{\mu_j}{j}, \mu_j = \left(\sum_{i=1}^j |\beta_{(i)}| - r\right)_+\}.$$

We denote the above transform by $f(\beta) = (t, s, \mu)$, which will be shown in the theory section is one-to-one, hence we can denote the inverse function as f^{-1} and use the change-of-variable method to compute the probability kernel for $\pi_{t,s,\mu|r}(t, s, \mu)$.

Theorem 1 (volume preserving transformation). *With $(t, s, \mu) = f(\beta)$ defined as the above, for any proper density π_β , the absolute determinant of the Jacobian, denoted by $|J_f|$, is one. Therefore,*

$$\pi_\beta(\beta) = \pi_{t,s,\mu|r}[f(\beta)].$$

Remark 2. *The constant $|J_f| = 1$ shows that f is a volume-preserving transform, hence the induced kernel is invariant to the number of non-zeros c . This is especially useful for the posterior computation, as the posterior kernel is continuous even when the number of zeros changes from c to c' .*

Step (ii) produces a sparse θ via the signed zero-thresholding $\theta_i = s_i(t_i)_+$. Equivalently, we can view $\pi_\theta(\theta)$ as the marginal form for $\pi_{t,s,\mu}(t, s, \mu)$, summed over those $(s_i, t_i) : t_i < 0$ and $\mu > 0$:

$$\begin{aligned} \pi_{\theta|r}(\theta) &= \pi_{\theta|r}(\theta_i = s_i t_i \text{ for } i \in C; \theta_i = 0 \text{ for } i \notin C) \\ &= \sum_{s_i = \pm 1 \text{ for } i \notin C} \int_0^\infty \int_{(-\mu/c, 0)^{p-c}} \pi_{t,s,\mu|r}(t, s, \mu) dt_{[p] \setminus C} d\mu. \end{aligned}$$

To show the details of the above results, we use a working example: consider an independent double exponential $\beta_i \sim \text{DE}(0, \lambda_i)$, $\pi(\beta_i) = 1/(2\lambda_i) \exp(-|\beta_i|/\lambda_i)$, with $\lambda_i > 0$. Transforming β to (t, s, μ) , we obtain the prior kernel:

$$\pi_{t,s,\mu|r}(t, s, \mu) = \prod_{i=1}^p \frac{1}{2\lambda_i} \exp\left(-\frac{\mu/c}{\lambda_i}\right) \exp\left(-\frac{t_i}{\lambda_i}\right), \quad (4)$$

subject to constraints $t_i > -\mu/c$ and $\sum_{i=1}^p (t_i)_+ = r$. In this special case, we can take a step further and integrate out $t_i : i \in [p] \setminus C$:

$$\begin{aligned} \text{pr}(\theta_i = 0) &= 1 - \exp\left(-\frac{\mu/c}{\lambda_i}\right), \quad \text{pr}(|\theta_i| > 0) = \exp\left(-\frac{\mu/c}{\lambda_i}\right), \\ \pi_\theta(\theta_i \mid |\theta_i| > 0) &= \frac{1}{2\lambda_i} \exp\left(-\frac{|\theta_i|}{\lambda_i}\right). \end{aligned} \quad (5)$$

Remark 3. To clarify, in this article, we choose to present the double exponential π_β for the ease of integration, which is useful for a tractable theoretic analysis later. In practice, we can choose any continuous π_β , such as the multivariate Gaussian. The volume preserving property and convenient computation will hold in general.

In general, the above marginal kernel may not be available in closed-form for other choice of π_β or more general $\mathbb{B}_{h,r}$, however, we can use the data augmentation (Tanner and Wong, 1987) for the posterior estimation. To elaborate, let $\mathcal{L}(y; \theta, \eta)$ be the likelihood, y the data, η some other parameter, we can sample the posterior β, r and η via:

$$\pi(\beta, \eta, r \mid y) \propto \pi_{\eta|\beta}(\eta) \pi_r(r) \pi_\beta(\beta) \mathcal{L}[y; P_{\mathbb{B}_{h,r}}(\beta), \eta]. \quad (6)$$

This means, we can first obtain the posterior samples of (η, r, β) , compute $\theta = P_{\mathbb{B}_{h,r}}(\beta)$ for each sample of β , then discard the other information.

2.4 Generalized l_1 -ball Prior

We now discuss the general cases that use l_1 -ball projection to create priors such that some transform of θ is sparse. Specifically, let $h : \mathbb{R}^p \rightarrow \mathbb{R}^d$, we use the following projection:

$$\theta = P_{\mathbb{B}_{h,r}}(\beta) = \underset{z \in \mathcal{Z} : \|h(z)\|_1 \leq r}{\operatorname{argmin}} \|z - \beta\|_2^2. \quad (7)$$

For regularities, we require $\|h(z)\|_1$ to be convex and \mathcal{Z} to be a convex set in \mathbb{R}^p . When these conditions are satisfied, the level set $\{z : \|h(z)\|_1 \leq r\}$ is a convex set, making the Euclidean projection unique hence a measurable transform. This includes a large class of useful functions, such as $h(z) = Dz$ with $D \in \mathbb{R}^{d \times p}$ as in the sparse contrast models, and $\|h(z)\|_1 = \sum_k \sqrt{\sum_j z_{k(j)}^2}$ as in the grouped shrinkage, $\operatorname{tr}[(ZZ^T)^{1/2}]$ as the nuclear norm to control the number of non-zero eigenvalues for square matrix Z . Further, we can consider \mathcal{Z} as a low-dimensional constrained space such as the one for positive definite matrix, for example, for modeling a sparse covariance/precision matrix.

The projection may not have a closed-form solution, however, it can be efficiently calculated using the splitting technique:

$$\theta = \underset{z : h(z)=s, \|s\|_1 \leq r}{\operatorname{argmin}} \|z - \beta\|_2^2 + \eta^T [h(z) - s] + \frac{1}{2\rho} \|h(z) - s\|_2^2,$$

where $\rho > 0$ and $\eta \in \mathbb{R}^d$ is Lagrangian multiplier (the values of ρ and η do not impact the convergence). Using $\kappa = \rho\eta$, the optimal solution can be computed using the alternating direction method of multipliers (ADMM) algorithm (Boyd et al., 2011), that iterates in:

$$\begin{aligned} z &\leftarrow \underset{z \in \mathcal{Z}}{\operatorname{argmin}} [\|z - \beta\|_2^2 + \frac{1}{2\rho} \|h(z) - s + \kappa\|_2^2], \\ s &\leftarrow P_{\mathbb{B}_r}[h(z) + \kappa], \\ \kappa &\leftarrow \kappa + h(z) - s, \end{aligned} \quad (8)$$

until it converges, and then set θ to be equal to z . Note that this algorithm contains a projection step to the vector-norm l_1 -ball, as in (2).

It is important to point out that, even though $P_{\mathbb{B}_{h,r}}(\beta)$ may not have a closed-form, $P_{\mathbb{B}_{h,r}}(\beta)$ is a continuous function of β , and differentiable almost surely with respect to the distribution of β , as explained in the next section.

2.5 Prior Specification on the Radius

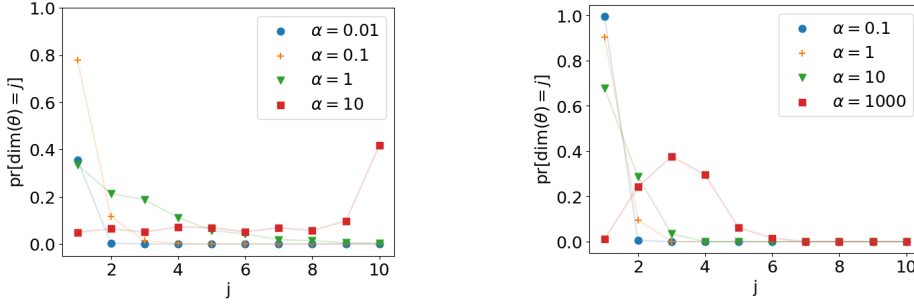
We now discuss how to choose π_r for the radius r . To induce a principled choice in simple linear models and to allow a straightforward prior calibration in complex models, we propose to use an exponential prior:

$$\pi_r(r) = \frac{1}{\alpha} e^{-r/\alpha},$$

with $\alpha > 0$ a calibration parameter chosen based on either some theory-guided conditions, or some prior assumption on the dimensionality of θ .

As we will show in the theory section, for the vector-norm l_1 -ball prior, with an exponential π_r and $\beta_i \sim \text{DE}(0, \lambda)$, we can obtain a closed-form expression on the cardinality of θ : $\text{pr}(|C| = j \mid \lambda, \alpha) = \lambda/\alpha(1 + \lambda/\alpha)^{-j}$ for $j = 1, \dots, (p-1)$. The tractable form enables us to choose α via the asymptotic theory of signal recovery in linear models.

For general cases involving other forms of π_β or l_1 -balls defined via $\|h(\theta)\|_1$, one can easily use numerical simulations to plot the induced prior distribution for the dimension of θ , varying according to the value of α . This allows one to calibrate α according to their prior belief. To illustrate this approach, in Figure 2 we show the prior distribution of the dimension of θ , for the vector-norm l_1 -ball prior based on normal $\beta_i \stackrel{\text{iid}}{\sim} N(0, 1)$ for a 10-dimensional vector β ; and the one of the dimension of matrix θ (rank) for the nuclear-norm l_1 -ball prior based on normal $\beta_{i,j} \stackrel{\text{iid}}{\sim} N(0, 1)$, $i \leq j$ for a 10×10 symmetric matrix β .



(a) Plotting $\text{pr}[\text{dim}(\theta) = j \mid \alpha]$ against j , with θ a 10-dimensional vector and α ranging from $\{0.01, 0.1, 1, 10\}$.

(b) Plotting $\text{pr}[\text{dim}(\theta) = j \mid \alpha]$ against j , with θ a 10×10 matrix and α ranging from $\{0.1, 1, 10, 1000\}$.

Figure 2: Prior distribution of $\text{dim}(\theta)$ with varying α . Panel (a) shows the cardinality of a vector with vector-norm l_1 -ball prior, and panel (b) shows the rank of a symmetric matrix with nuclear-norm l_1 -ball prior.

3 Continuous Hamiltonian Monte Carlo for Posterior Computation

The Hamiltonian Monte Carlo is a powerful method for sampling the posterior distribution. It uses the Hamiltonian dynamics to propose a new state of parameter and accept it using the Metropolis-Hastings criterion. Due to the energy-preserving property, the Hamiltonian dynamics is capable of producing a proposal that is far away from the current state, while often enjoying a high acceptance rate. Neal (2011) provides an introduction on this algorithm.

One limitation, however, is that the common algorithm in the Hamiltonian Monte Carlo (such as the one implemented in Stan) only works on the continuous random variable under a continuous posterior density. Although some data augmentation methods are proposed for the binary discrete random variable, such as Pakman and Paninski (2013), they create discontinuity in the augmented posterior. To briefly explain, when a binary variable changes from 0 to 1, the likelihood will have a sudden jump that breaks the energy-preserving property of Hamiltonian dynamics. To handle this issue, one needs a modified algorithm such as the discontinuous Hamiltonian Monte Carlo (Nishimura et al., 2020).

Interestingly, the l_1 -ball priors (including the generalized l_1 -ball priors) are free from this issue, as long as π_β is continuous in β and the likelihood is continuous in θ . Intuitively, for the l_1 -ball prior, as β_i reduces in magnitude, θ_i gradually changes toward 0 and stays at 0 after passing below the threshold — therefore, the projection function is continuous. We now formalize this intuition using the property of the proximal mapping, then briefly explain the Hamiltonian Monte Carlo algorithm.

3.1 Almost Sure Smoothness of the Posterior

We first introduce the concept of the proximal mapping (for a more comprehensive introduction, see Beck (2017)), defined as

$$\text{prox}_g(x) = \underset{z}{\operatorname{argmin}} \{g(z) + \|x - z\|_2^2/2\},$$

with g a lower-semicontinuous and convex function. Now we choose $g = \mathcal{X}_{\mathbb{B}_{h,r}}$, the characteristic function of a set (an l_1 -ball), which takes value 0 in $\mathbb{B}_{h,r}$ and takes ∞ otherwise. Since $\mathbb{B}_{h,r}$ is a convex set, this means that the projection $P_{\mathbb{B}_{h,r}}(\beta)$ is a proximal mapping.

As a useful property, the proximal mapping is Lipschitz continuous with the Lipschitz constant 1 (Beck (2017), Theorem 6.42); in our case,

$$\|P_{\mathbb{B}_{h,r}}(\beta_1) - P_{\mathbb{B}_{h,r}}(\beta_2)\|_2 \leq \|\beta_1 - \beta_2\|_2.$$

Further, by the Rademacher’s Theorem (Federer (2014), Thm. 3.1.6), any Lipschitz continuous function is differentiable almost everywhere with respect to the measure on its input — in our case, the chosen π_β before the projection.

As a result, when the likelihood function is continuous in θ , it is continuous in β using variable transformation $\theta = P_{\mathbb{B}_{h,r}}(\beta)$, hence the posterior is a continuous function of β as well. Further, if the likelihood is smooth with respect to θ almost surely, then the posterior is smooth almost surely as well. Therefore we can simply run the continuous Hamiltonian Monte Carlo (HMC). We provide a brief review of the HMC algorithm and describe further details of implementing this algorithm in the supplementary materials.

3.2 Point Estimate and Credible Region for the Low Dimensional Parameter

Uncertainty quantification often relies on the calculation of the credible region: for a certain function of the random variable $g(\theta)$ (such as θ itself, fitted value $X\theta$, etc.), we want a region R_g , such that

$$\text{pr}[g(\theta) \in R_g \mid y] = 1 - \tilde{\alpha},$$

with some given $\tilde{\alpha} \in (0, 1)$.

A common way to approximate R_g is to take the posterior samples of $g(\theta)$, and take point-wise quantiles in the elements of the $g(\theta)$ output, while adjusting for multiplicity. However, this

is sub-optimal for a sparse θ and/or an intrinsically low-dimensional $g(\theta)$ (such as the piece-wise linear $X\theta$), for two reasons: (i) the multiplicity adjustment is often too conservative, making the credible region too large (that is, the associated probability is in fact much larger than $1 - \tilde{\alpha}$); (ii) the combination of the point-wise credible intervals is often no longer low-dimensional.

To bypass these issues, we use the solution from Breth (1978) based on the *top* $(1 - \tilde{\alpha})$ posterior density region:

$$R_g = \{g(\theta) : \pi_\theta(\theta | y) \geq \kappa_{\tilde{\alpha}}\},$$

where $\kappa_{\tilde{\alpha}}$ is a threshold that makes the region having a probability $1 - \tilde{\alpha}$. In practice, we can approximate $\kappa_{\tilde{\alpha}}$ by simply calculating the posterior kernels for all the samples, then taking the $\tilde{\alpha}$ quantile.

Similarly, for a point estimate, since θ may reside on a low-dimensional space \mathcal{M} , the sample mean of θ or $g(\theta)$ is not ideal as it may end up being high-dimensional. Therefore, we use the Fréchet mean:

$$\overline{g(\theta)} = \arg \min_{g(z): z \in \mathcal{M}} \mathbb{E}_{\theta \sim \pi(\theta|y)} \|g(z) - g(\theta)\|^2.$$

As we often do not know \mathcal{M} , we can approximate the above using the posterior samples $\{\theta^j\}_{j=1 \dots m}$, which give the estimator $\arg \min_{g(z): z \in \{\theta^j\}} \sum_{\theta \in \{\theta^j\}} \|g(z) - g(\theta)\|^2$. We will illustrate these in numerical examples.

4 Theoretical Study on l_1 -ball Prior

We now focus on a more theoretical study on the l_1 -ball prior. For ease of analysis, we focus on the vector-norm l_1 -ball in this section.

First, we show that the augmented transform f in the l_1 -projection is indeed invertible. Recall that $f : \mathbb{R}^p \rightarrow \{(t, s, \mu) \in \mathbb{R}^p \times \{1, -1\}^p \times \mathbb{R}_+ : \sum_{i=1}^p (t_i)_+ = r, t_i \geq -\mu/|C|\}$.

Theorem 2. Consider another transform $\beta = g(t, s, \mu)$ with $C = \{i : t_i > 0\}$, and let

$$\beta_i = s_i(t_i + \frac{\mu}{|C|}), \quad (9)$$

where its domain satisfies the following: $s_i \in \{-1, 1\}$; if $\sum_{i \in C} t_i = r$, then for $i \notin C$, $-\mu/|C| \leq t_i \leq 0$ and $\mu \geq 0$; if all $t_i \geq 0$ and $\sum t_i < r$, then $\mu = 0$. If $|C| = 0$, all $\beta_i = 0$. Then g is the inverse mapping of f , that is:

$$f[g(t, s, \mu)] = (t, s, \mu), \quad g[f(\beta)] = \beta.$$

Remark 4. Broadly speaking, this gives an “projection-based data augmentation” scheme for any sparse θ : we can augment (t_i, s_i) ’s for those $\theta_i = 0$ and a $\mu \geq 0$, and then apply $\beta = g(t, s, \mu)$. The produced β is a continuous embedding for θ .

Next, we establish a link between some special form of the l_1 -ball prior to the combinatorial prior that chooses a subset of θ to be zero. When $\beta_i \stackrel{\text{iid}}{\sim} \text{DE}(0, \lambda)$, we can further integrate and obtain two simple marginal forms.

Theorem 3. If $\pi_\beta(\beta) = \prod_i (2\lambda)^{-1} \exp(-|\beta_i|/\lambda)$ with $\lambda > 0$, then for $\theta \in \text{int}\mathbb{B}_r$, $\pi_{\theta|r, \lambda}(\theta) = \prod_i (2\lambda)^{-1} \exp(-|\theta_i|/\lambda) \mathbb{I}(\|\theta\|_1 < r)$, and for $\theta \in \text{bd}\mathbb{B}_r$,

$$\pi_{\theta|r, \lambda}(\theta) = \frac{(2\lambda)^{-|C|}}{\binom{p}{|C|}} \lambda \exp\left(-\frac{r}{\lambda}\right) \mathbb{I}(\|\theta\|_1 = r), \quad (10)$$

where $C = \{i \in [p] : \theta_i \neq 0\}$.

Further marginalizing over θ on $\{\theta : \|\theta\|_1 = r, \sum_{i=1}^p \mathbb{I}(\theta_i \neq 0) = j\}$, we can obtain a discrete prior distribution on $|C|$.

Corollary 1. *If $\pi_\beta(\beta) = \prod_i (2\lambda)^{-1} \exp(-|\beta_i|/\lambda)$ with $\lambda > 0$, then the marginal prior $\pi(|C|; r)$ follows a truncated Poisson distribution, with*

$$\text{pr}(|C| = j \mid r) = \frac{(r/\lambda)^{j-1}}{(j-1)!} \exp\left(-\frac{r}{\lambda}\right), \quad (11)$$

for $j = 1, \dots, (p-1)$; and $\text{pr}(|C| = p \mid r) = 1 - \sum_{j=1}^{p-1} (r/\lambda)^{j-1}/(j-1)! \exp(-r/\lambda)$.

In the above, we can see how the radius impacts the level of sparsity:

$$\begin{aligned} \mathbb{E}(|C| - 1) &= \sum_{j=1}^{p-1} (j-1) \frac{(r/\lambda)^{j-1}}{(j-1)!} \exp\left(-\frac{r}{\lambda}\right) + (p-1) \sum_{j=p}^{\infty} \frac{(r/\lambda)^{j-1}}{(j-1)!} \exp\left(-\frac{r}{\lambda}\right) \\ &\leq r/\lambda, \end{aligned}$$

where the inequality is due to $(p-1) \leq (j-1)$ for $j \geq p$ and the expectation of an untruncated Poisson (r/λ) is r/λ . Therefore, a smaller r favors a smaller $|C|$ and more θ_i 's to be zero.

Lastly, we study the posterior convergence rate using the above prior. Since the rate is highly dependent on the form of the likelihood, we choose to narrow our focus on the well-studied linear regression model, and demonstrate an equivalently optimal rate as the existing approaches. For a comprehensive review on this topic, see Castillo and van der Vaart (2012).

We follow the standard theoretic analysis and assume y_i and θ_i are re-scaled by $1/\sigma$, so that $y_i \sim N(x_i^T \theta, 1)$, while assuming there is an oracle $\theta^0 \in \mathbb{R}^p$, with the true cardinality $c_0 \neq 0$. In practice, since we do not know σ^2 we can assign a prior on $\sigma^2 \sim \text{Inverse-Gamma}(\gamma_{\sigma^2,1}, \gamma_{\sigma^2,2})$, and additionally let θ scale with σ . To provide a straightforward result, we use $\pi_r(r) = \alpha^{-1} \exp(-r/\alpha)$ with α a parameter to determine. Multiplying it to (11) and integrating over r , and we obtain the marginal model selection probability under the $\pi_r(r)$:

$$\text{pr}(|C| = j; \lambda, \alpha) = \frac{\lambda/\alpha}{(1 + \lambda/\alpha)^j}, \quad (12)$$

for $j = 1, \dots, (p-1)$; and $\text{pr}(|C| = p; \lambda, \alpha) = 1 - \sum_{j=1}^{p-1} \lambda/\alpha (1 + \lambda/\alpha)^{-j} = (1 + \lambda/\alpha)^{-(p-1)}$. And

$$\pi_\theta(\theta) = \frac{(2\lambda)^{-|C|}}{\binom{p}{|C|}} \lambda/\alpha \exp\left[-(1/\lambda + 1/\alpha)^{-1} \|\theta\|_1\right], \quad (13)$$

for $|C| = 1, \dots, (p-1)$.

Remark 5. *The equations (12) and (13) show that, even after marginalizing over the radius r , the prior still has a positive probability for θ to contain $k = p - |C|$ zeros.*

We now present the convergence result.

Theorem 4. *If the data are generated from $y_i = X_{i,\cdot} \theta^0 + \epsilon_i$, $\epsilon_i \stackrel{iid}{\sim} N(0, 1)$, with (λ, α) chosen as $\lambda = b_1 p^{b_2} / \|X\|_{2,\infty}$, $\alpha = p^{b_3} / \|X\|_{2,\infty}$, $b_1 > 0$, $b_2 > b_3$, $b_3 \leq 1$, and $\|X\|_{2,\infty} := \max_j \sqrt{\sum_i X_{i,j}^2}$, with sufficiently large M , then as $n, p \rightarrow \infty$:*

- (Cardinality) For estimating the true cardinality c_0 ,

$$\sup_{\theta^0} \mathbb{E}_{\theta^0} \pi \left(\theta : |C_\theta| > c_0 \left[1 + \frac{M}{b_2 - b_3} \left(1 + \frac{16}{\phi(C_0)^2} \frac{\lambda^*}{2\|X\|_{2,\infty}\sqrt{\log p}} \right) \right] \middle| y \right) \rightarrow 0,$$

where $\lambda^* = \|X\|_{2,\infty}(b_1 p^{b_2} + p^{b_3})/(b_1 p^{b_2} p^{b_3})$.

- (l_2 -recovery) The recovery of true θ^0 has

$$\sup_{\theta^0} \mathbb{E}_{\theta^0} \pi \left(\theta : \|\theta - \theta^0\|_2 > \frac{M}{\psi(C_0)^2} \frac{\sqrt{c_0 \log p}}{\|X\|_{2,\infty} \phi(C_0)} \middle| y \right) \rightarrow 0,$$

- (l_1 -recovery) The recovery of true θ^0 has

$$\sup_{\theta^0} \mathbb{E}_{\theta^0} \pi \left(\theta : \|\theta - \theta^0\|_1 > \frac{M}{\bar{\psi}(C_0)^2} \frac{c_0 \sqrt{\log p}}{\|X\|_{2,\infty} \phi(C_0)^2} \middle| y \right) \rightarrow 0.$$

- (l_∞ -recovery) For every $\eta > 0$, any $d_0 < \eta^2 [1 + 2/(b_2 - b_3)]^{-1}/8$, and c_n such that $c_n(b_1 p^{b_2} + p^{b_3})\sqrt{\log p}/(b_1 p^{b_2} p^{b_3}) \rightarrow 0$, for the set $\mathcal{C}^* = \{C_0 : \phi(C_0) \geq \eta, \psi(C_0) \geq \eta, c_0 \leq c_n, c_0 \leq d_0 mc(X)^{-1}\}$, then the recovery of true θ^0 has

$$\sup_{\theta^0 : C_0 \in \mathcal{C}^*} \mathbb{E}_{\theta^0} \pi \left(\theta : \|\theta - \theta^0\|_\infty > M \frac{\sqrt{\log p}}{\|X\|_{2,\infty}} \middle| y \right) \rightarrow 0.$$

In the above, $mc(X) = \max_{i \neq j} \frac{|X_{:,i}^T X_{:,j}|}{\|X_{:,i}\|_2 \|X_{:,j}\|_2}$ is the mutual coherence, and $\phi(C), \bar{\psi}(C), \psi(C)$ are the compatibility numbers for matrix X that we give the definitions in the supplementary materials.

Taking one step further, we now characterize the uncertainty via examining the asymptotic posterior distribution in linear regression. For a given model $C \subset [p]$, we let X_C be the $n \times |C|$ subset matrix consisting of the columns $X_{:,i}$ with $i \in C$, and $\hat{\theta}_C$ be the least square estimator in the restricted model $\hat{\theta}_C \in \operatorname{argmin}_{\theta_C \in \mathbb{R}^{|C|}} \|Y - X_C \theta_C\|_2$. We obtain the following Bernstein von-Mises theorem, which shows the posterior converging to a Gaussian distribution concentrated on the true model when $n \rightarrow \infty$.

Theorem 5. Let (λ, α) be chosen as $\lambda = b_1 p^{b_2}/\|X\|_{2,\infty}, \alpha = p^{b_3}/\|X\|_{2,\infty}$ with $b_1 > 0, b_2^{-1} = o_p(1), b_3 \leq 1$, and we assume θ^0 is in the parameter space $\Theta^0 = \{\theta^0 : |\theta_i^0| \geq \frac{M}{\bar{\psi}(C_0)^2} \frac{c_0 \sqrt{\log p}}{\|X\|_{2,\infty} \phi(C_0)^2} \forall i \in C_0\}$, with sufficiently large $M; c_0 \sqrt{\log p}/\|X\|_{2,\infty} \rightarrow 0; \phi(C_0) \geq a_0; \bar{\psi}(C_0) \geq a_0; \tilde{\sigma}_{\min}(X_{C_0}^T X_{C_0})/\|X\|_{2,\infty} \geq a_0\}$ with $\tilde{\sigma}_{\min}(\cdot)$ denotes the smallest eigenvalue of a matrix. Then for any $a_0 > 0$, as $n, p \rightarrow \infty$:

$$\sup_{\theta^0 \in \Theta^0} \|\pi(\theta | Y) - N(\hat{\theta}_{C_0}, (X_{C_0}^T X_{C_0})^{-1}) \otimes \delta_{[p] \setminus C_0}\|_{TV} \rightarrow 0,$$

where $\delta_{[p] \setminus C_0}$ denotes the Dirac measure at a zero vector for those $\theta_i : i \notin C_0$.

Remark 6. To justify the assumptions about Θ^0 , the first condition is that the absolute value of each non-zero entry in θ^0 is larger than a threshold; the second condition and the positive lower bound on ϕ and $\bar{\psi}$ make this threshold go to zero when $p \rightarrow \infty$; the last condition on the first eigenvalue ensures the positive definiteness of $X_{C_0}^T X_{C_0}$.

5 Comparison with Some Existing Methods

5.1 Comparison with the Spike-and-Slab Priors

The spike-and-slab priors are well known for solving Bayesian variable selection problems, and they are also capable of inducing exact zeros in θ with a positive probability. Therefore, we provide a detailed comparison between the l_1 -ball and the spike-and-slab priors.

As there are multiple variants under the name of spike-and-slab, we focus on the ones in the following form (Lempers, 1971; Mitchell and Beauchamp, 1988):

$$\begin{aligned} (\theta_i | \tau_i) &\stackrel{\text{indep}}{\sim} (1-w)\delta_0(\cdot) + w\delta_{\tau_i}(\cdot), \\ \tau_i &\stackrel{\text{iid}}{\sim} \pi_\tau, \end{aligned} \tag{14}$$

for $i = 1, \dots, p$, where $\delta_x(\cdot)$ denotes a point mass at point x , and π_τ denotes a continuous distribution centered at zero such as Gaussian $N(0, \sigma_\tau^2)$, $w \in (0, 1)$ is a probability, typically assigned with a beta prior. Therefore, this prior is a two-component mixture of point mass at 0 (“spike”) and a continuous distribution π_τ (“slab”). The later versions (George and McCulloch, 1995; Ishwaran and Rao, 2005) improve the computational performance by replacing 0 with another continuous distribution concentrated near zero; however, they lose the positive probability at zero. Therefore, for a direct comparison with the l_1 -ball prior, we will focus on the Lempers-Mitchell-Beauchamp version here.

On the one hand, we show that the classic spike-and-slab prior can be in fact viewed as a special case of the l_1 -ball prior, under three restrictions: (i) isotropic Π_β , (ii) projection to a vector l_1 -norm ball, (iii) quantile-based threshold. We now construct an l_1 -ball prior that has the same marginal form as (14). Consider a distribution for β isotropic in each coordinate/element and dependent on w :

$$\begin{aligned} \beta_i &\stackrel{\text{iid}}{\sim} \pi_{\tilde{\tau}}, \\ \pi_{\tilde{\tau}}(x; w) &= \begin{cases} (1-w)\pi_0(x), & \text{if } |x| \leq \tilde{\mu} \\ w\pi_\tau[\text{sign}(x)(|x| - \tilde{\mu})_+], & \text{if } |x| > \tilde{\mu} \end{cases}, \end{aligned} \tag{15}$$

where $\pi_0(x)$ is an augmented density that accounts for the probability of producing $\theta_i = 0$, and we can use any proper density that integrates to 1 and has support over $[-\tilde{\mu}, \tilde{\mu}]$, with $\tilde{\mu} > 0$ determined by the choice of $\pi_0(x)$.

Using the *soft-thresholding* representation $\theta_i = \text{sign}(\beta_i)(|\beta_i| - \tilde{\mu})_+$, it is not hard to see that we have $\theta_i = 0$ with probability $1-w$, and $\theta_i \sim \pi_\tau$ if $\theta_i \neq 0$, independently for $i = 1, \dots, p$. Therefore, this distribution is marginally equivalent to (14).

Based on this connection, we can use continuous Hamiltonian Monte Carlo for the posterior computation under a spike-and-slab prior. In the supplementary materials, we show that empirically, this leads to much faster mixing performance in the Markov chains, compared to the conventional combinatorial search based on the update of binary inclusion variables.

On the other hand, by relaxing those restrictions, the l_1 -ball prior and the generalized l_1 -ball prior can induce a much more flexible model than the spike-and-slab — in particular, those zero elements $\theta_i = 0$ (the “spikes”) no longer need to be independent, but can satisfy some complicated dependence and/or combinatorial constraints as we motivated in the beginning.

First, we can easily induce dependence among the zeros in θ by replacing the isotropic π_β with a correlated one. For example, using $\beta \sim N(0, \Sigma_\beta)$, we can see that, after the projection,

$$\text{pr}(\theta_i = \theta_{i'} = 0) = \text{pr}(|\beta_i| \leq \tilde{\mu}, |\beta_{i'}| \leq \tilde{\mu}),$$

which is the probability for finding a correlated bivariate Gaussian random variable inside a box $[-\tilde{\mu}, \tilde{\mu}]^2$ — if their correlation is close to 1, then when $\theta_{i'}$ is zero, θ_i is very likely to be zero as well. This could be very useful if one wants to impose prior assumption on where the zeros could simultaneously appear. In the numerical experiments, we will show an example of inducing dependence with a correlated π_β in a brain connectivity study.

Second, by replacing the vector norm $\|\theta\|_1$ with more general $\|h(\theta)\|_1$ we can now induce sparsity on a constrained or low-dimensional space, such as the sparse contrast and reduced-dimension examples we presented early. Such a task would be very difficult to do via (14), for two reasons (i) assigning an element-wise spike-and-slab prior on a constrained parameter would create an intractable normalizing constant (that involves the parameter w and the ones in π_τ), making the prior specification/calibration very difficult; (ii) the computation would become formidably challenging, due to the need to satisfy the constraints when updating the value of each θ_i [hence early methods tend to rely on approximation, such as Banerjee and Ghosal (2013) for estimating sparse covariance matrix]. To compare, the l_1 -ball prior does not have these issues since the prior is fully defined on the unconstrained parameter β without any intractable constant, and we can easily sample from the posterior distribution.

5.2 Comparison with the Post-processing Algorithms

There are several works in the literature on post-processing continuous posterior samples to obtain exact zeros (Bondell and Reich, 2012; Hahn and Carvalho, 2015; Li and Pati, 2017). In the supplementary materials, we provide a detailed comparison of both methodology and numerical experiments on point estimates.

6 Numerical Experiments

In this section, we illustrate three interesting applications related the motivating combinatorial problems as described in Section 2.1.

6.1 Sparse Contrast Modeling: Piece-wise Constant Smoothing

In the first example, we conduct a task of image denoising/segmentation. Consider each pixel measurement of an image as $y_{i,j} \in \mathbb{R}$ (for simplicity, we focus on one color channel) modeled by:

$$y_{i,j} = \mu + \theta_{i,j} + \varepsilon_{i,j}, \quad \varepsilon_{i,j} \stackrel{\text{iid}}{\sim} N(0, \sigma^2),$$

for all pixels indexed by horizontal $i = 1, \dots, p_1$ and vertical $j = 1, \dots, p_2$ and some scalar $\mu \in \mathbb{R}$. A common strategy is to impose segment-wise (piece-wise) constant $\theta_{i,j}$'s as a smoothing for the image, nevertheless, the issue is that the boundary of each segment is not predefined; hence finding the boundary of and the number of segments is a combinatorial problem.

A nice solution, popularized by the fused lasso (Tibshirani et al., 2005), is to induce sparsity in contrasts:

$$\theta_{i,j} - \theta_{i+1,j}, \quad \theta_{i,j} - \theta_{i,j+1}$$

for $i = 1, \dots, p_1 - 1$ and $j = 1, \dots, p_2 - 1$; as well as sparsity in $\theta_{i,j}$'s. Applying l_1 -norm on each and summing up, we can represent the regularization by $\|D\theta\|_1$, with matrix $D \in \mathbb{R}^{d \times (p_1 p_2)}$ and $d = (p_1 - 1)p_2 + p_1(p_2 - 1) + p_1 p_2$.

Besides point estimate, a common inference task is to assess whether a non-zero difference across the boundary is indeed significant, or just random variation. A popular frequentist solution is to develop a series of hypothesis tests [for recent work, see Jewell et al. (2022) and references

within]. On the other hand, using our l_1 -ball prior based on $\mathbb{B}_{h,r}$ with $h(\theta) = D\theta$, we can obtain a simple Bayesian solution. Using the ADMM algorithm we described in (8), we have the first step in closed-form:

$$z \leftarrow [(2\rho)^{-1}D^T D + I]^{-1}[\beta + (2\rho)^{-1}D^T(s - \kappa)],$$

hence the projection of β to $\theta \in \mathbb{B}_{h,r}$ can be evaluated rapidly.

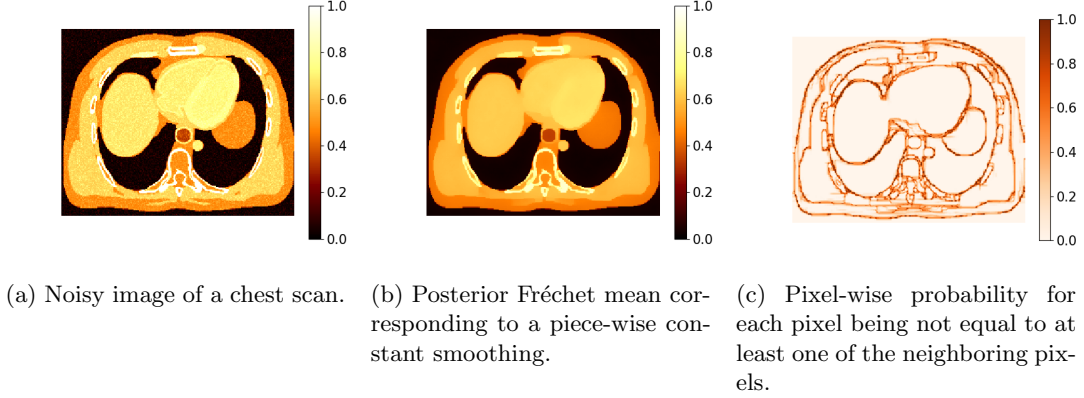


Figure 3: An example of the sparse contrast modeling using the generalized l_1 -ball prior. Our model finds a piece-wise constant smoothing (b) underneath a noisy image (a), while quantifying the uncertainty (c).

We apply the above model with a generalized l_1 -ball prior using $\beta_{i,j} \stackrel{\text{iid}}{\sim} \text{DE}(0, 1)$, and $\alpha = 10$. The scan image is from Gong et al. (2017) and previously used by Xu and Fan (2021), with the noisy raw data plotted in Figure 3(a). In the posterior samples, the Fréchet mean indeed recovers a segment-wise constant structure, with each part clearly shown (b). Importantly, we quantify the posterior probability that a smoothed pixel is not equal to at least one of its neighbors, $\text{pr}[\theta_{i,j} \neq \theta_{(i+k,j+k')}]$ for at least one $(k, k') = (0, 1), (1, 0), (-1, 0), (0, -1) \mid y]$ for $i = 2, \dots, p-1$ and $j = 2, \dots, p-1$. Indeed, those large probabilities are located near the boundary; and interesting extension could be further explored, such as one for Bayesian multiplicity control on image boundary detection.

6.2 Reduced Dimension Modeling: Finding the Number of Mixture Components

To illustrate the usefulness of exact zeros outside the linear models, we consider the prior specification problem for the finite mixture model. We focus on the K -component Gaussian mixture likelihood:

$$\pi(y_j; \theta, \mu, \sigma^2) = \sum_{k=1}^K \theta_k \phi(y_j \mid \mu_k, \sigma_k^2),$$

for $j = 1, \dots, n$, where $\phi(\cdot \mid a, b)$ denotes the normal density with the mean a and variance b .

Suppose the data are generated from a K_0 -component model, but we do not know K_0 exactly; hence a common Bayesian modeling practice is to assign a prior on the θ_k 's and shrink some of them close to zero. For example, it has been popular to use the infinite mixture model, which considers K as unbounded and assigns a stick-breaking construction on $\{\theta_k\}_{k=1}^\infty$, such as

the one in the Dirichlet process. However, this was recently discovered to yield an inconsistent result (Miller and Harrison, 2014) for the number of components, as the posterior probability $\text{pr}(K = K_0)$ goes to zero as $n \rightarrow \infty$. Later, Miller and Harrison (2018) show that instead of putting an infinite mixture prior on θ_k , if we treat K as a finite number and put a prior $\Pi_K(K)$, this can yield a consistent estimation at K_0 . They refer to it as the “mixture of finite mixtures” model. The major drawback is that this involves a combinatorial search over different K ’s.

Using the l_1 -ball prior, we can significantly simplify this problem. Assuming we know a K_1 large enough to have $K_1 > K_0$, starting from $\beta_i \stackrel{\text{ind}}{\sim} \text{DE}(0, \lambda_i)$, we project it to the l_1 -ball and apply the transformation:

$$w = P_{\mathbb{B}_r}(\beta), \quad \theta_k = \frac{|w_k|}{\sum_{i=1}^{K_1} |w_i|} \text{ for } k = 1, \dots, K_1,$$

note that in the second step, we have $\sum_{i=1}^{K_1} |w_i| = r$ if $\sum_{i=1}^{K_1} |\beta_i| \geq r$. Compared to the parameter space in an infinite mixture model $\{\theta : \theta_k > 0 \ \forall k \in \mathbb{Z}_+, \sum_{k=1}^{\infty} \theta_k = 1\}$, besides being finite dimensional, a key difference here is that the space of θ is the *closure* of the probability simplex (which includes the case for some $\theta_k = 0$),

$$\Delta^{K_1-1} = \{\theta : \theta_k \geq 0 \ \forall k, \sum_{k=1}^{K_1} \theta_k = 1\},$$

Therefore, using the projection, we assign a positive probability for each $K \in \{1, \dots, K_1\}$; hence this gives a continuous version of the mixture of finite mixtures model.

When simulating the data, we use $K_0 = 3$ with $(0.3, 0.3, 0.4)$ as the mixture weights; to have the components overlap, we use $\mu_1 = 0, \mu_2 = 4, \mu_3 = 6$, and all $\sigma_1^2 = \sigma_2^2 = \sigma_3^2 = 1$. We generate $n = 1,000$ in the simulation.

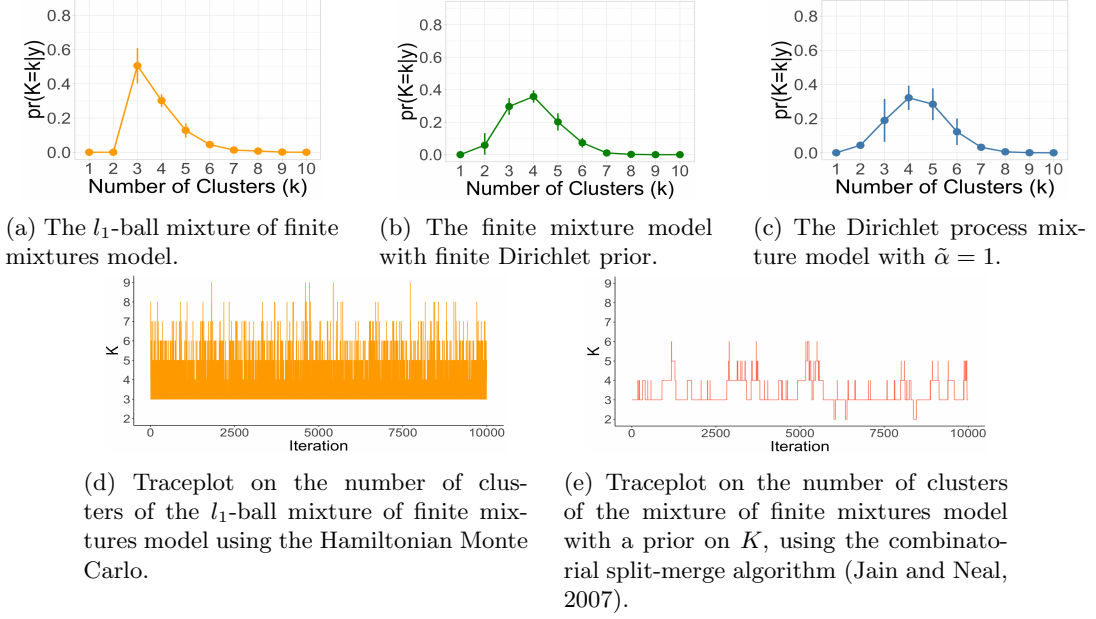


Figure 4: Comparing the performances of applying l_1 -ball prior to the finite mixture weight and the other mixture models. The experiment is repeated five times, and the mean of the number of clusters with its standard error is presented. In each experiment, we run the Markov chain for 20,000 iterations and discard the first 10,000 as burn-ins.

For the l_1 -ball prior, we use $K_1 = 10$, Inverse-Gamma(1, 1) prior for σ_k^2 and $N(0, 10^2)$ prior for μ_k . To compare, we also use (i) the Dirichlet process mixture model with the concentration parameter $\tilde{\alpha} = 1$; (ii) the finite mixture model with the same dimension $K_1 = 10$, but with a finite Dirichlet distribution prior $(\theta_1, \dots, \theta_{K_1}) \sim \text{Dir}(\tilde{\alpha})$ with $\tilde{\alpha} = 0.001$ to favor sparsity in θ . We use the same prior for μ_k and σ_k^2 ; for the radius prior in the l_1 -ball prior, we use $\alpha = 3$.

Figure 4 shows the posterior distribution of K in all three models. Clearly, the one uses the l_1 -ball has the largest probability assigned to $K_0 = 3$. Both the Dirichlet process mixture model and the finite mixture model with a Dirichlet prior put the largest probability at $K = 4$. The good result is because we effectively assign a discrete prior on the number of mixture components, hence the consistency theory of Miller (2022) directly applies. In addition, we compare the computing performance using the l_1 -ball prior against the combinatorial search using the split-merge algorithm (Jain and Neal, 2007). The l_1 -ball mixture of finite mixtures enjoys faster mixing and less autocorrelation.

6.3 Nonlinear Modeling: Discontinuous Gaussian Process Regression

Gaussian process regression is a useful non-parametric method to model nonlinear functions. For outcome $y_i \in \mathbb{R}$ and predictors $x_i \in \mathbb{R}^p$, we model the outcome

$$y_i = f(x_i) + \epsilon_i, \quad \epsilon_i \stackrel{\text{iid}}{\sim} N(0, \sigma_\epsilon^2), \quad f(x) \sim GP[0, K_\theta(\cdot, \cdot)]$$

for $i = 1, \dots, n$, where GP represents a Gaussian process, such that any finite dimensional realization follows a multivariate normal with mean 0 vector and covariance determined by the covariance function $\text{Cov}[f(x_i), f(x_j)] = K_\theta(x_i, x_j)$. An often seen property of those popular covariance

functions, such as squared exponential and Matérn, is that the correlation $\text{Corr}[f(x_i), f(x_j)] \rightarrow 1$ as $\|x_i - x_j\|_2 \rightarrow 0$; as the result, it imposes almost everywhere continuity: for every $\delta_1 > 0$, there is a δ_2 such that for any $(x_i, x_j) : \|x_i - x_j\|_2 \leq \delta_2 \Rightarrow |f(x_i) - f(x_j)| \leq \delta_1$. This continuity may not be desirable, if we want to model f as a function containing one or several points of discontinuity. To address this shortcoming, Gramacy and Lee (2008) proposed to use multiple independent Gaussian processes, each supported on one of the partitioned regions; to obtain the partition, they used a predictor-partition tree that requires a combinatorial search in the computation.

We now develop a simple alternative that uses one Gaussian process, based on a slight modification of a popular squared exponential covariance function, and an application of a generalized l_1 -ball prior. With a predictor-dependent graph $\mathcal{G} = (\mathcal{V}, \mathcal{E}_x)$ with \mathcal{V} containing n nodes, and edges formed by radial neighbors $\mathcal{E}_x = \{(i, j) : \|x_i - x_j\|_2 \leq d\}$ with some pre-set d (we choose the smallest d so that each node has at least one connected neighbor on \mathcal{G}), we use $\theta = \{\sigma_K^2, \lambda_1, \lambda_2, \eta\}$ and specify

$$K_\theta(x_i, x_j) = \sigma_K^2 \exp\left[-\frac{\|x_i - x_j\|_2^2}{\lambda_1}\right] \exp\left[-\frac{|\eta_i - \eta_j|^2}{\lambda_2}\right],$$

$$\eta = P_{\{z: \sum_{(i,j) \in \mathcal{E}_x} |z_i - z_j| \leq r\}}(\beta), \quad \beta_i \stackrel{\text{iid}}{\sim} \text{DE}(0, 1),$$

where $\sigma_K^2 > 0$, $\lambda_1 > 0$, $\lambda_2 > 0$ are the parameters for a squared exponential covariance function. For the radius prior in the l_1 -ball prior, we use $\alpha = 0.1$. We put an Inverse-Gamma(2, 0.1) prior on each of those parameters. At the same time, we introduce $\eta_i \in \mathbb{R}$ as a *latent jittering coordinate*, that arises from a generalized l_1 -ball prior related to the graph-fused lasso (Tibshirani and Taylor, 2011). As the result of the projection, most of $(i, j) \in \mathcal{E}_x$ would have $\eta_i = \eta_j$; however, a few (i, j) would have $\eta_i \neq \eta_j$. On any edge with $\eta_i \neq \eta_j$, we have $\text{Corr}[f(x_i), f(x_j)] \ll 1$ even if $x_i \approx x_j$, which allows discontinuity to occur.

We use the above model in a political science data application. The data were collected from $n = 59$ voting districts. The goal is to find a relationship between the vote percentage for Party 1 and several predictors, including the vote share of Party 1 in the last election, minorities percentage in the voters, and urban percentage (Lee et al., 2004). Since we observe the vote percentages directly, we use their log-odds transforms as y_i 's and model them by Gaussian processes. The scatter plot in Figure 5(a) shows that there is a sudden jump in the current-year vote percentage when the vote share from the last election passes near 50%, which is likely due to the increased polarization of political preferences since the last election.

For a clear illustration, in the main text, we fit regression models using the vote share for Party 1 in the last election as the only predictor (the single predictor model allows the fitted curves to be smooth in x_i except for points of discontinuity). To compare, we also fit the regression models using the continuous Gaussian Process with a squared exponential covariance function. As shown in Figure 5(b) and (c), the discontinuous Gaussian process successfully discovers two distinct values in η_i 's and gives a better fit to the data, compared to the continuous one. The root-mean-square deviation (RMSD) is 0.478 for the discontinuous model, and 0.589 for the continuous one. When using all three predictors, the discontinuous Gaussian process finds three distinct values in η_i 's, and we provide the results and comparison in the supplementary materials.

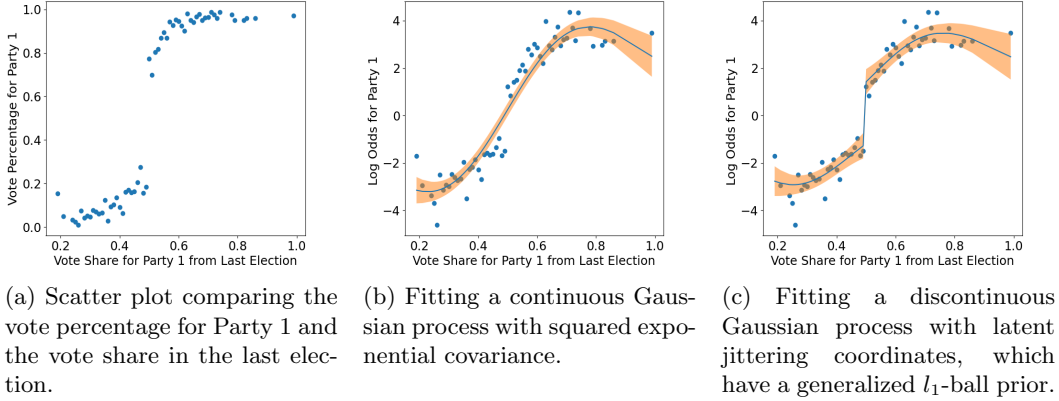


Figure 5: Discontinuous Gaussian process regression on the election data (Panel a). With a latent jittering coordinate η_i regularized by a generalized l_1 -ball prior, we can change a Gaussian process with squared exponential covariance function (Panel b) to have points of discontinuity (Panel c), giving an improved fit to the data. The fitted curves and 95% point-wise credible bands are shown.

6.4 Additional Numerical Results

In the supplementary materials, we provide some additional results related to (i) benchmarking the l_1 -ball prior method in linear regression setting; (ii) simulation in change point detection with comparison to continuous shrinkage prior; (iii) numerical comparison with post-processing methods on the accuracy of linear model selection; (iv) assessing the mixing performance of running Hamiltonian Monte Carlo via the l_1 -ball parameterization for a spike-and-slab prior, with comparison to the Gibbs sampling algorithm; (v) application of the l_1 -ball prior to induce structured sparsity; (vi) simulation on rank recovery with nuclear-norm l_1 -ball prior.

7 Data Application: Sparse Change Detection in the Medical Images

For the application, we use the l_1 -ball prior on the analysis of a medical imaging dataset. The data are the abdominal dynamic contrast-enhanced magnetic resonance imaging (Otazo et al., 2015), collected on a healthy human subject during normal breathing. It is in the form of a video, acquired via a whole-body scanner to record the aorta, portal vein and liver enhancement. There are 384×384 pixels in each frame (corresponding to 0.94 seconds) and $T = 75$ frames in total.

An important scientific task is to detect the locations of the large changes, corresponding to important organ activities. However, there are a few challenges: (i) most parts of the image are not fixed but also dynamically changing (such as the overall brightness, although to a less degree compared to the sharp changes), hence we need to model a “background” time series; (ii) the video is noisy hence there are uncertainties on the detected changes. To handle this problem, we consider the low-rank plus sparse model:

$$M_t = \sum_{k=1}^d \tilde{\alpha}_{t,k} \psi_k + S_t + E_t,$$

for $t = 1, \dots, T$; where the $\psi_k \in \mathbb{R}^{384 \times 384}$ corresponds to some latent component shared by all frames, and $\tilde{\alpha}_{t,k}$ is the loading dynamically changing over time; $S_t \in \mathbb{R}^{384 \times 384}$ is a sparse matrix corresponding to the sharp changes that we wish to detect; E_t corresponds to the noise and we model it as independent $N(0, \sigma_e^2)$ for each of its element.

A common problem for low-rank modeling is to determine the rank, in this case, the number of latent components d . Bhattacharya and Dunson (2011) previously proposed to view d as unbounded, while applying a continuous shrinkage prior on the scale of loading, closer towards zero as k increases. We are inspired by this idea, nevertheless, we achieve an exact rank selection by using a generalized l_1 -ball prior based on the nuclear norm. This has two advantages: we can treat the low-rank part using one matrix parameter L replacing $\sum_k \tilde{\alpha}_{t,k} \psi_k$, which avoids the potential identifiability issues when estimating $\tilde{\alpha}_{t,k}$ and ψ_k separately; having an exactly low-rank part reduces the confoundingness between the near-low-rank and sparse signals.

Specifically, we reparameterize the 75 matrices $\{\sum_{k=1}^d \tilde{\alpha}_{t,k} \psi_k\}_{t=1}^T$ via a single matrix of size 75×384^2 :

$$L = \sum_{k=1}^d (\tilde{\alpha}_{1,k}, \dots, \tilde{\alpha}_{T,k}) [\text{vec}(\psi_k)]^T.$$

Without specifying d , we can treat L as the output of projecting a dense matrix $\beta \in \mathbb{R}^{75 \times 384^2}$ to a generalized l_1 -ball:

$$L = \underset{Z \in \mathbb{R}^{75 \times 384^2} : \|Z\|_* \leq r}{\text{argmin}} \|Z - \beta\|_F^2$$

where $\|Z\|_*$ denotes the nuclear norm, as the sum of the singular values $\sum_{k=1}^{75} \rho_k(Z)$, with $Z = U_Z \text{diag}[\rho_k(Z)] V_Z^T$.

Since having exact $\rho_k(Z) = 0$ for some k 's will lead to an effective rank reduction to $d = |\{\rho_k(Z) : \rho_k(Z) > 0\}|$, the nuclear norm regularization is very popular in the optimization literature (Hu et al., 2012). This projection has a closed-form solution: if $\sum_k \rho_k(\beta) \geq r$, $L = U_\beta \text{diag}[(\rho_k(\beta) - \tilde{\mu})_+] V_\beta^T$, for some $\tilde{\mu} > 0$ such that $\sum_k [\rho_k(\beta) - \tilde{\mu}]_+ = r$; $L = \beta$ if $\sum_k \rho_k < r$. For the radius prior in the l_1 -ball prior, we use $\alpha = 100$.

Assigning $\beta_{i,j} \sim \text{DE}(0, \lambda_{i,j})$, we can quantify the uncertainty regarding the rank. Further, we assign an element-wise l_1 -ball prior to each element of S_t , so that we can obtain sparse estimates on the sharp changes. In the supplementary materials, we show that the background time series is mostly based on the linear combination of 2 latent components (panel a), each corresponding to a dense image (b-c). By visualizing the estimated backgrounds at three different time points, we can see some very subtle differences, such as the brightness between (d) and (f), which involves most of the pixels. Indeed, these small changes are what we wish to find and separate from the sparse part S_t .

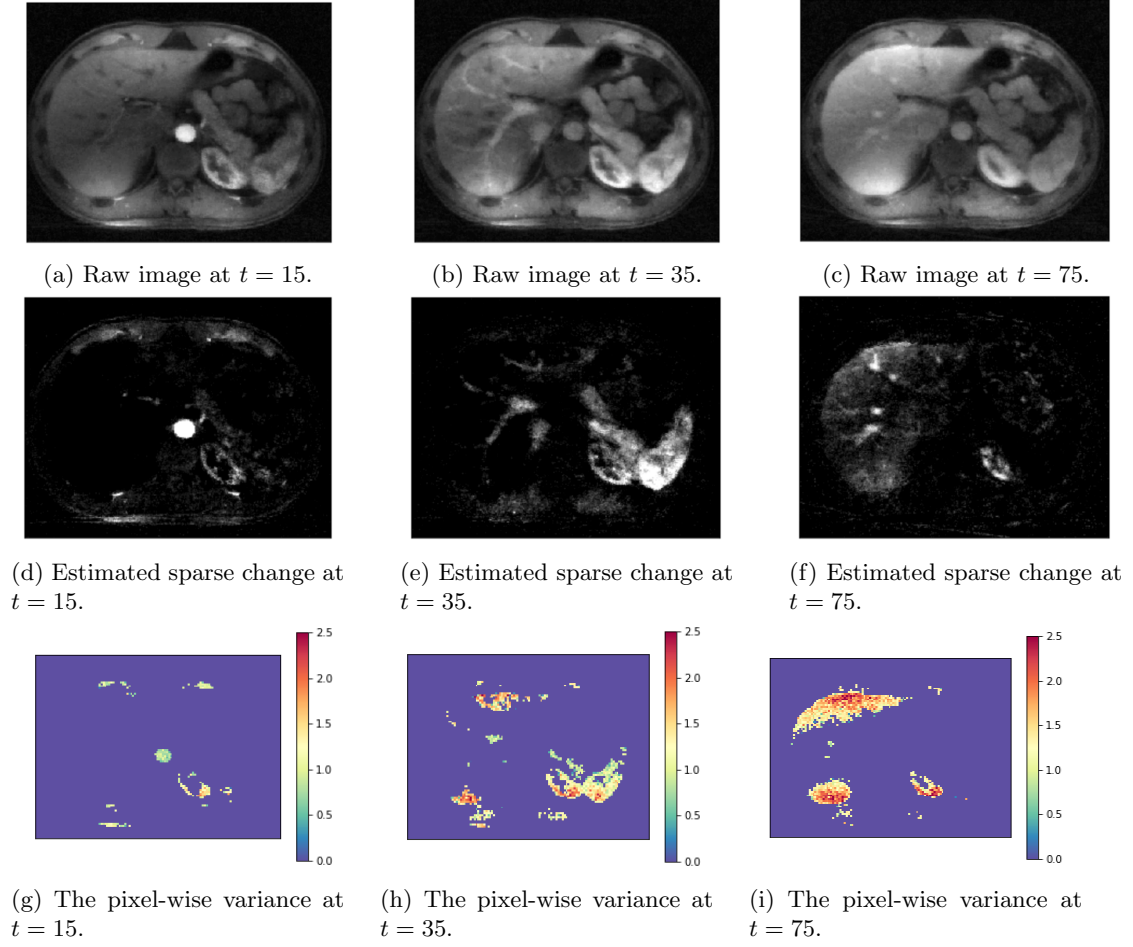


Figure 6: The sparse change component S_t and its pixel-wise variances are visualized. The three frames correspond to three time points, when the aorta, liver and portal vein are in their enhancement phase respectively. The posterior of the sparse parameter shows the locations of these changes, as well as the uncertainties.

Figure 6 shows the locations of the sharp changes we estimate from the sparse S_t . The results are very interpretable as they correspond to when the aorta, portal vein, and liver are in their enhancement phases, respectively. The vessels and organs are distinct from the abdominal background. Further, we compute the pixel-wise variance for these sparse estimates, as a measurement of the uncertainty. It can be seen that the aorta and portal vein (panels g and h) have a relatively low uncertainty on the changes; whereas the liver (panel i) has a higher uncertainty, hence some caution should be applied when making a conclusion based on the last frame. In the supplementary materials, we experiment with a simpler alternative that replaces the low-rank $\sum_{k=1}^d \tilde{\alpha}_{t,k} \psi_k$ with a time-invariant background ψ_0 . This leads to much less sparse estimates that are more difficult to interpret.

8 Discussion

In this article, we propose a new prior defined on the boundary of the l_1 -ball. This allows us to build many interesting applications that implicitly involve a combinatorial selection, such as in the change points, the number of mixture components and the rank of a matrix. We show that the l_1 -ball projection is continuous hence giving a convenient “continuous embedding” for these combinatorial problems, establishing a connection between the rich optimization and Bayesian literature.

There are several interesting extensions worth pursuing. First, when projecting a continuous distribution into the boundary of a certain geometric set, it often leads to a degenerate distribution that is useful but difficult to parameterize directly. This convenient property is not limited to the l_1 -ball. For example, in the high-dimensional optimal transport problem, when estimating the contingency probability table given two marginal probability vectors, the solution table is likely to be very sparse (Cuturi, 2013). This is due to the projection to the high-dimensional polytope will likely end up in the vertex corresponding to a high sparsity. Therefore, our projection idea can be generalized to such useful geometric sets. Second, our data augmentation strategy can be viewed as “augmentation-by-optimization”, as opposed to the conventional “augmentation-by-integration”. Polson and Scott (2016) have previously explored the connection and difference between maximizing and integrating over a latent variable, under the scope of comparing a frequentist/optimization-based model and its Bayesian counterpart; here, we demonstrate that the barrier can be in fact removed, and the Bayesian models can leverage a maximization over a certain latent variable, creating a new class of useful priors. Lastly, for the theory, we chose to focus on linear regression because of the tractability of vector-norm l_1 -ball projection, and we can analytically integrate out several parameters to obtain a simple combinatorial prior; for generalized l_1 -ball projection, a direct analysis would be difficult hence it is interesting to explore different strategies.

Supplementary Materials

A Proofs

Proof. Since permutation of indices does not affect $|J|$, without loss of generality, we assume $\sum_{i=1}^c |\theta_i| = r$ and $|\theta_i| > 0$ for $i = 1, \dots, c$.

Now f^{-1} is a mapping from $(\theta_1, \dots, \theta_{c-1}, t_{c+1}, \dots, t_p, \mu)$ to $(\beta_1, \dots, \beta_{c-1}, \beta_{c+1}, \dots, \beta_p, \beta_c)$, where $\beta_c = s_c(r - \sum_{i=1}^{c-1} |\theta_i| + \mu/c)$. The Jacobian matrix J is

$\frac{\partial}{\partial \theta_1}$	β_1	\dots	β_{c-1}	β_{c+1}	\dots	β_p	β_c
	1	\dots	0	0	\dots	0	$-s_1 s_c$
\vdots	\vdots	\ddots	\vdots	\vdots	\vdots	\vdots	\vdots
$\frac{\partial}{\partial \theta_{c-1}}$	0	\dots	1	0	\vdots	0	$-s_{c-1} s_c$
$\frac{\partial}{\partial t_{c+1}}$	0		0	s_{c+1}	0	0	0
\vdots	\vdots	\vdots	\vdots	\vdots	\ddots	\vdots	\vdots
$\frac{\partial}{\partial t_p}$	0	\dots	0	0	\dots	s_p	0
$\frac{\partial}{\partial \mu}$	s_1/c	\dots	s_{c-1}/c	s_{c+1}/c	\dots	s_p/c	s_c/c

Split the matrix into four blocks, with $A = J_{1:(p-1), 1:(p-1)}$, $B = J_{p, 1:(p-1)}$, $C = J_{1:(p-1), p}$ and

$D = s_c/c$. We know

$$\begin{aligned}
|J| &= |D - BA^{-1}C||A| \\
&= |s_c/c + \sum_{i=1}^{c-1} s_i^2 s_c/c| \times 1 \\
&= |s_c| \\
&= 1.
\end{aligned}$$

□

Proof of Theorem 2

Proof. With β_i 's re-ordered $|\beta_{(1)}| \geq \dots \geq |\beta_{(p)}|$, we will prove $|\beta_{(j)}| > (\sum_{i=1}^j |\beta_{(i)}| - r)/j$ for all $j \leq |C|$ and $|\beta_{(j)}| < (\sum_{i=1}^j |\beta_{(i)}| - r)/j$ for $j > |C|$. This is equivalent to comparing $(j-1)|\beta_{(j)}| - (\sum_{i=1}^{j-1} |\beta_{(i)}| - r)$ against 0.

When $j \leq |C|$,

$$\begin{aligned}
&(j-1)|\beta_{(j)}| - (\sum_{i=1}^{j-1} |\beta_{(i)}| - r) \\
&= (j-1)(|\theta_{(j)}| + \frac{\mu}{|C|}) - \{ \sum_{i=1}^{j-1} (|\theta_{(i)}| + \frac{\mu}{|C|}) - r \} \\
&= (j-1)|\theta_{(j)}| - (\sum_{i=1}^{j-1} |\theta_{(i)}| - r) \\
&> 0,
\end{aligned}$$

since $\sum_{i=1}^{j-1} |\theta_{(i)}| < r$ for $j \leq |C|$.

When $j > |C| + 1$,

$$\begin{aligned}
&(j-1)|\beta_{(j)}| - (\sum_{i=1}^{j-1} |\beta_{(i)}| - r) \\
&= (j-1)(t_{(j)} + \frac{\mu}{|C|}) - \left\{ \sum_{i=1}^{|C|} (|\theta_{(i)}| + \frac{\mu}{|C|}) + \sum_{i=|C|+1}^{j-1} (t_{(i)} + \frac{\mu}{|C|}) - r \right\} \\
&= (j-1)t_{(j)} - \left\{ \sum_{i=1}^{|C|} |\theta_{(i)}| + \sum_{i=|C|+1}^{j-1} t_{(i)} - r \right\} \\
&\stackrel{(a)}{=} (j-1)t_{(j)} - \sum_{i=|C|+1}^{j-1} t_{(i)} \\
&\stackrel{(b)}{<} (j-1-|C|)t_{(j)} - \sum_{i=|C|+1}^{j-1} t_{(i)} \\
&= \sum_{i=|C|+1}^{j-1} (t_{(j)} - t_{(i)}) \\
&\stackrel{(c)}{\leq} 0,
\end{aligned}$$

where (a) is due to $\sum_{i=1}^{|C|} |\theta_{(i)}| = r$, (b) due to $t_{(j)} < 0$ and (c) due to $|\beta_{(j)}| - \mu/|C| \leq |\beta_{(i)}| - \mu/|C|$ for $j > i$.

When $j = |C| + 1$, $(j - 1)|\beta_{(j)}| - (\sum_{i=1}^{j-1} |\beta_{(i)}| - r) = |C|t_{(j)} < 0$.

Therefore, we have $c = |C|$, and it can be verified that

$$\mu_c = \sum_{i=1}^{|C|} (|\theta_{(i)}| + \frac{\mu}{|C|}) - r = \mu.$$

□

Proof of Theorem 3

Proof. For ease of notation, we denote $\vec{t}_{\bar{C}} := t_{\sigma_1}, \dots, t_{\sigma_{p-|C|}}$

$$\begin{aligned} \pi_{\theta}(\theta) &= \sum_{\substack{s_{\sigma_1}, \dots, s_{\sigma_{p-|C|}} \\ \in \{-1, 1\}^{p-|C|}}} \int_0^{\infty} \int_{(-\mu/|C|, 0)^{p-|C|}} \pi_{\beta}\{g(t, s, \mu)\} d\vec{t}_{\bar{C}} d\mu \\ &= 2^{p-|C|} (2\lambda)^{-p} \int_0^{\infty} \int_{(-\mu/|C|, 0)^{p-|C|}} \prod_{i \in \bar{C}} \left\{ e^{-\frac{|\theta_i| + \mu/|C|}{\lambda}} \right\} \prod_{i \in \bar{C}} \left\{ e^{-\frac{t_i + \mu/|C|}{\lambda}} \right\} d\vec{t}_{\bar{C}} d\mu \\ &= 2^{p-|C|} (2\lambda)^{-p} \prod_{i \in \bar{C}} \left\{ \exp\left(-\frac{|\theta_i|}{\lambda}\right) \right\} \int_0^{\infty} e^{-\frac{p\mu}{\lambda|C|}} \int_{(-\mu/|C|, 0)^{p-|C|}} \prod_{i \in \bar{C}} e^{-\frac{t_i}{\lambda}} d\vec{t}_{\bar{C}} d\mu \\ &= 2^{p-|C|} (2\lambda)^{-p} \exp\left(-\frac{r}{\lambda}\right) \cdot \lambda^{p-|C|} \int_0^{\infty} e^{-\frac{p\mu}{\lambda|C|}} \left(e^{\frac{\mu}{\lambda|C|}} - 1 \right)^{p-|C|} d\mu. \end{aligned}$$

Let $u = e^{-\frac{\mu}{\lambda|C|}}$, then $du = -(\lambda|C|)^{-1} e^{-\frac{\mu}{\lambda|C|}} d\mu$, we have

$$\int_0^{\infty} e^{-\frac{p\mu}{\lambda|C|}} \left(e^{\frac{\mu}{\lambda|C|}} - 1 \right)^{p-|C|} d\mu = \lambda|C| \int_0^1 u^{|C|-1} (1-u)^{p-|C|} du = \lambda \frac{\Gamma(|C|+1) \Gamma(p-|C|+1)}{\Gamma(p+1)}.$$

Combining the results,

$$\pi_{\theta}(\theta) = \frac{(2\lambda)^{-|C|}}{\binom{p}{|C|}} \lambda \exp\left(-\frac{r}{\lambda}\right)$$

□

Proof of Corollary 1

Proof. We first focus on when $\|\theta\|_1 < r$, since under which, $|C| < p$ happens with probability zero, therefore,

$$\begin{aligned}
\text{pr}(|C| = p, \|\theta\|_1 < r) &= \int_{\mathbb{R}^p} \prod_i (2\lambda)^{-1} \exp(-|\theta_i|/\lambda) \mathbb{I}(\|\theta\|_1 < r) d\theta \\
&= \int_{\mathbb{R}_+^p} \prod_i (\lambda)^{-1} \exp(-x_i/\lambda) \mathbb{I}(\sum x_i < r) dx \\
&\stackrel{(a)}{=} \int_0^r \frac{1}{\Gamma(p)\lambda^p} y^{p-1} \exp(-y/\lambda) dy \\
&\stackrel{(b)}{=} 1 - \sum_{j=0}^{p-1} \frac{1}{j!} \left(\frac{r}{\lambda}\right)^j \exp(-r/\lambda),
\end{aligned}$$

where (a) uses the fact that sum of p iid $\text{Exp}(\lambda)$'s is a $\text{Gamma}(p, \lambda)$ with λ the scale parameter, and (b) uses the CDF formula as p is an integer.

When $\|\theta\|_1 = r$, and $|C| = j$, denote the non-zero indices by $\{i_1, \dots, i_j\}$, note that $x = (|\theta_{i_1}|/r, \dots, |\theta_{i_j}|/r)$ is on a probability simplex with dimension $(j-1)$, Δ^{j-1} , hence we can use Dirichlet distribution integral $\int_{\Delta^{j-1}} 1 dx = 1/\Gamma(j)$. We have

$$\begin{aligned}
\text{pr}(|C| = j, \|\theta\|_1 = r) &= \frac{(2\lambda)^{-j}}{\binom{p}{j}} \lambda \exp\left(-\frac{r}{\lambda}\right) 2^j \binom{p}{j} r^{j-1} / \Gamma(j) \\
&= \left(\frac{r}{\lambda}\right)^{j-1} \exp\left(-\frac{r}{\lambda}\right) / (j-1)!,
\end{aligned}$$

for $j = 1, \dots, p$. Combining the above gives the result. \square

Proof of Theorem 4

Proof. The compatibility numbers are

$$\begin{aligned}
\phi(C) &= \inf_{\theta} \left\{ \frac{\|X\theta\|_2 |C|^{1/2}}{\|X\|_{2,\infty} \|\theta\|_1} : \|\theta_{[p] \setminus C}\|_1 \leq 7 \|\theta_C\|_1, \theta_C \neq 0 \right\}, \\
\psi(C) &= \tilde{\phi} \left[\left(2 + \frac{3}{a+b} + \frac{33}{\phi(C)^2} \frac{\lambda^*}{2\|X\|_{2,\infty} \sqrt{\log p}} \right) |C| \right], \\
\bar{\psi}(C) &= \bar{\phi} \left[\left(2 + \frac{3}{a+b} + \frac{33}{\phi(C)^2} \frac{\lambda^*}{2\|X\|_{2,\infty} \sqrt{\log p}} \right) |C| \right], \\
\tilde{\phi}(c) &:= \inf_{\theta} \left\{ \frac{\|X\theta\|_2}{\|X\|_{2,\infty} \|\theta\|_2} : 0 \neq |C_\theta| \leq c \right\} \\
\bar{\phi}(c) &:= \inf_{\theta} \left\{ \frac{\|X\theta\|_2 |C_\theta|^{1/2}}{\|X\|_{2,\infty} \|\theta\|_1} : 0 \neq |C_\theta| \leq c \right\}.
\end{aligned}$$

Our results are based on the early work of Castillo et al. (2015), Theorems 1 and 2: For a constant λ^* and a discrete distribution $g(c)$ supported on $\{0, \dots, p\}$, when

$$1. \quad \|X\|_{2,\infty}/p \leq \lambda^* \leq 4\|X\|_{2,\infty} \sqrt{\log p},$$

2. There exist constants $a_1, a_2, a_3, a_4 > 0$ with (2.2) $a_1 p^{-a_3} \leq \frac{g(c)}{g(c-1)} \leq a_2 p^{-a_4}$ for $c = 2, \dots, p$.

Then for a prior kernel of the form

$$\pi_\theta(\theta; \lambda^*, g) = g(|C|) \frac{1}{\binom{p}{|C|}} \left(\frac{\lambda^*}{2}\right)^{|C|} \exp(-\lambda^* \|\theta\|_1),$$

with $g(|C| = j) = \text{pr}(|C| = j)$, would enjoy the results in the theorem. We now check these two conditions and compute the associated constants.

Using the chosen λ and α , we have

$$\lambda^* = \frac{\lambda + \alpha}{\lambda \alpha} = \|X\|_{2,\infty} \frac{b_1 p^{b_2} + p^{b_3}}{b_1 p^{b_2} p^{b_3}},$$

Since $b_3 \leq 1$, we have $\lambda^* \geq \|X\|_{2,\infty}/p^{b_3} \geq \|X\|_{2,\infty}/p$. Since $b_2 > b_3$, for p large enough, $b_1 p^{b_2} > p^{b_3}$, hence $\|X\|_{2,\infty}(b_1 p^{b_2} + p^{b_3})/(b_1 p^{b_2} p^{b_3}) \leq 2/p^{b_3} \|X\|_{2,\infty} \leq 4\|X\|_{2,\infty} \sqrt{\log p}$.

On the other hand, When $c = 1, \dots, p-1$.

$$\frac{g(c)}{g(c-1)} = (1 + \lambda/\alpha)^{-1} = \frac{1}{1 + b_1 p^{b_2 - b_3}}.$$

Clearly, $g(c)/g(c-1) \leq 1/(b_1 p^{b_2 - b_3})$, satisfying $a_2 = 1/b_1$ and $a_4 = b_2 - b_3$. For p large enough $b_1 p^{b_2 - b_3} > 1$, we have $g(c)/g(c-1) \geq 1/(2b_1 p^{b_2 - b_3})$, satisfying $a_1 = 1/(2b_1)$ and $a_3 = b_2 - b_3$. When $c = p$, $g(c)/g(c-1) = \alpha/\lambda = 1/(b_1 p^{b_2 - b_3})$, hence also satisfying the above results. Therefore, we apply $a_4 = b_2 - b_3$ in the two theorems of Castillo et al. (2015), and arrive at our results. \square

Proof of Theorem 5

Proof. Let π_1 denote the restricted normal distribution under the true model $N(\hat{\theta}_{C_0}^0, (X_{C_0}^T X_{C_0})^{-1}) \otimes \delta_{[p] \setminus C_0}$, and

$$\pi_2(\theta) = (2\pi)^{(c_0 - |C_\theta|)/2} \frac{|X_{C_0}^T X_{C_0}|^{1/2}}{|X_{C_\theta}^T X_{C_\theta}|^{1/2}} e^{-\frac{1}{2}(\|Y - X_{C_\theta} \theta_{C_\theta}\|_2^2 - \|Y - X_{C_0} \theta_{C_0}\|_2^2 + \|X_{C_\theta} \hat{\theta}_{C_\theta}\|_2^2 - \|X_{C_0} \hat{\theta}_{C_0}\|_2^2)},$$

$$\pi_3(\theta) = \frac{\pi_\theta(\theta)}{\pi_\theta(\theta^0)}.$$

Thus, the posterior $\pi(\theta | Y) \propto \pi_1 \pi_2 \pi_3$. Let A be the set

$$\left\{ \theta : |C_\theta| \leq c_0 \left[1 + \frac{M}{b_2 - b_3} \left(1 + \frac{16}{\phi(C_0)^2} \frac{\lambda^*}{2\|X\|_{2,\infty} \sqrt{\log p}} \right) \right], \right. \\ \left. \text{and } \|\theta - \theta^0\|_1 \leq \frac{M}{\bar{\psi}(C_0)^2} \frac{c_0 \sqrt{\log p}}{\|X\|_{2,\infty} \phi(C_0)^2} \right\}.$$

By Theorem 4, $\pi(A | Y) \rightarrow 1$ under \mathbb{P}_{θ^0} . We now prove that $\pi_1(A | Y) \rightarrow 1$ under \mathbb{P}_{θ^0} as well. Let

$Z \sim N(\hat{\theta}_{C_0}^0, (X_{C_0}^T X_{C_0})^{-1}) \otimes \delta_{[p] \setminus C_0}$, then Z immediately satisfies $|C_Z| \leq c_0 \left[1 + \frac{M}{b_2 - b_3} \left(1 + \frac{16}{\phi(C_0)^2} \frac{\lambda^*}{2\|X\|_{2,\infty} \sqrt{\log p}} \right) \right]$.

Denote $B_n = \frac{M}{\bar{\psi}(C_0)^2} \frac{c_0 \sqrt{\log p}}{\|X\|_{2,\infty} \phi(C_0)^2}$. We have

$$\begin{aligned}
\Pr(\|Z - \theta^0\|_1 \leq B_n) &= \Pr(\|Z_{C_0} - \hat{\theta}_{C_0} + \hat{\theta}_{C_0} - \theta_{C_0}^0\|_1 \leq B_n) \\
&= \Pr(\|(X_{C_0}^T X_{C_0})^{-1} X_{C_0}^T (\varepsilon + \eta)\|_1 \leq B_n) \\
&\geq \Pr(\text{tr}[(X_{C_0}^T X_{C_0})^{-1}] \|\varepsilon + \eta\|_2 \leq B_n) \\
&\geq \Pr(c_0 [\tilde{\sigma}_{\min}(X_{C_0}^T X_{C_0})]^{-1} \|\varepsilon + \eta\|_2 \leq B_n) \\
&\geq \Pr\left(\|\varepsilon + \eta\|_2 \leq \frac{M}{\bar{\psi}(C_0)^2} \frac{\sqrt{\log p}}{\phi(C_0)^2} \tilde{\sigma}_{\min}(X_{C_0}^T X_{C_0})\right) \\
&\geq \Pr\left(\|\varepsilon + \eta\|_2 \leq \frac{M}{\bar{\psi}(C_0)^2} \frac{\sqrt{\log p}}{\phi(C_0)^2} a_0\right) \rightarrow 1,
\end{aligned}$$

where ε and η are two independent standard normal vectors in \mathbb{R}^n . The second equality holds because both $Z_{C_0} - \hat{\theta}_{C_0}$ and $\hat{\theta}_{C_0} - \theta_{C_0}^0$ follows $N(0, (X_{C_0}^T X_{C_0})^{-1})$, and the first inequality holds due to Cauchy-Schwarz inequality.

Since the total variation distance between a probability measure $\pi(\cdot)$ and its renormalized restriction $\pi_A(\cdot) = \pi(\cdot)/\pi(A)$ is bounded above by $2\pi^c(A)$, we can replace the two measures in the total variation distance by their renormalized restrictions to A . Therefore, it is sufficient to show

$$\int_A |\pi_1 \pi_2 \pi_3 - N(\hat{\theta}_{C_0}^0, (X_{C_0}^T X_{C_0})^{-1}) \otimes \delta_{[p] \setminus C_0}| d\theta \rightarrow 0.$$

We now show that $\max_{\theta \in A} |\pi_2(\theta) - 1| \rightarrow 0$ and $\max_{\theta \in A} |\pi_3(\theta) - 1| \rightarrow 0$, where we need to firstly prove $\pi(C_\theta = C_0 | Y) \rightarrow 1$ for $\theta \in A$. By Theorem 4, we have

$$\sum_{C_0 \subseteq C} \pi(\theta : C_\theta = C | y) \leq \pi(\|\theta - \theta^0\|_1 > \frac{M}{\bar{\psi}(C_0)^2} \frac{c_0 \sqrt{\log p}}{\|X\|_{2,\infty} \phi(C_0)^2} | Y) \rightarrow 0.$$

Therefore $\pi(C_\theta \supseteq C_0 | Y) \rightarrow 1$. In light of assertion 1 in Theorem 4 and the choice of λ , we have $\pi(|C_\theta| \leq c_0 | Y) \rightarrow 1$. Combining the last two conclusion, we have $\pi(C_\theta = C_0 | Y) \rightarrow 1$. Then

$$\begin{aligned}
\|Y - X_{C_\theta} \theta_{C_\theta}\|_2^2 - \|Y - X_{C_0} \theta_{C_0}\|_2^2 &\leq \|X_{C_\theta \setminus C_0} \theta_{C_\theta \setminus C_0}\|_2^2 + 2(Y - X_{C_0} \theta_{C_0})^T X_{C_\theta \setminus C_0} \theta_{C_\theta \setminus C_0} \\
&\leq \|X_{C_\theta \setminus C_0} \theta_{C_\theta \setminus C_0}\|_2^2 + 2\|\varepsilon\|_2 \|X_{C_\theta \setminus C_0} \theta_{C_\theta \setminus C_0}\|_2 \rightarrow 0 \text{ in probability.}
\end{aligned}$$

Since $\|X_{C_\theta} \hat{\theta}_{C_\theta}\|_2^2 - \|X_{C_0} \hat{\theta}_{C_0}\|_2^2$ is the square length of the projection of Y on a subspace of dimension $|C_\theta| - c_0$, this also converge to 0 in probability, hence $\max_{\theta \in A} |\pi_2(\theta) - 1| \rightarrow 0$.

Since

$$\pi_3(\theta) = (2\lambda)^{c_0 - |C_\theta|} \frac{\binom{p}{C_0}}{\binom{p}{C_\theta}} \exp[-(1/\lambda + 1/\alpha)(\|\theta\|_1 - \|\theta^0\|_1)],$$

and that $|\|\theta\|_1 - \|\theta^0\|_1| \leq \|\theta - \theta^0\|_1 \leq \frac{M}{\bar{\psi}(C_0)^2} \frac{c_0 \sqrt{\log p}}{\|X\|_{2,\infty} \phi(C_0)^2} \rightarrow 0$, we have $\max_{\theta \in A} |\pi_3(\theta) - 1| \rightarrow 0$.

Combining the above results, we have

$$\begin{aligned}
& \int_A |\pi_1 \pi_2 \pi_3 - N(\hat{\theta}_{C_0}^0, (X_{C_0}^T X_{C_0})^{-1}) \otimes \delta_{[p] \setminus C_0}| d\theta \\
&= \int_A |\pi_1 \pi_2 \pi_3 + \pi_1 \pi_2 - \pi_1 \pi_2 - \pi_1| d\theta \\
&\leq \int_A |\pi_1 \pi_2 - \pi_1| d\theta + \int_A |\pi_1 \pi_2 (\pi_3 - 1)| d\theta \\
&\leq \max_{\theta \in A} |\pi_2 - 1| \int_A |\pi_1| d\theta + \max_{\theta \in A} |\pi_3 - 1| \int_A |\pi_1 \pi_2| d\theta \rightarrow 0.
\end{aligned}$$

□

B Review of the HMC Algorithm

For completeness, we now briefly review the Hamiltonian Monte Carlo (HMC) algorithm. To sample the parameter $q = (\beta, \eta, r)$ from target distribution $q \sim \pi_{q|y}(\cdot)$, the HMC algorithm takes an auxiliary momentum variable v with density $\pi_v(v)$, and samples from the joint distribution $\pi(q, v) = \pi_{q|y}(q) \pi_v(v)$. The potential energy and kinetic energy are defined as $U(q) = -\log \pi_{q|y}(q)$ and $K(v) = -\log \pi_v(v)$, and the total Hamiltonian energy function is denoted by $H(q, v) = U(q) + K(v)$. Our choice of $\pi_v(v)$ is the multivariate Gaussian density $N(0, I)$, with the kinetic energy $K(v) = v^T v / 2$.

At each state (q, v) , a new proposal is generated by simulating Hamiltonian dynamics, which satisfy Hamilton's equations:

$$\frac{\partial q}{\partial t} = \frac{\partial H(q, v)}{\partial v} = v, \quad \frac{\partial v}{\partial t} = -\frac{\partial H(q, v)}{\partial q} = -\frac{\partial \log \pi_{q|y}(q)}{\partial q}. \quad (16)$$

The exact solution for (16) is often intractable, but we can numerically approximate the solution to the differential equations by algorithms such as the leapfrog scheme. The leapfrog is a reversible and volume-preserving integrator, which updates the evolution $(q^{(t)}, v^{(t)}) \rightarrow (q^{(t+\epsilon)}, v^{(t+\epsilon)})$ via

$$v \leftarrow v + \frac{\epsilon}{2} \frac{\partial \log \pi_{q|y}(q)}{\partial q}, \quad q \leftarrow q + \epsilon v, \quad v \leftarrow v + \frac{\epsilon}{2} \frac{\partial \log \pi_{q|y}(q)}{\partial q}. \quad (17)$$

The proposal (q^*, v^*) is generated by taking L leapfrog steps from current state $(q^{(0)}, v^{(0)})$, then accepted using the Metropolis-Hastings adjustment, with the acceptance probability:

$$\min\{1, \exp[-H(q^*, v^*) + H(q^{(0)}, v^{(0)})]\}.$$

For the step size ϵ and the leapfrog steps L , we use the No-U-Turn Sampler (Hoffman and Gelman, 2014) to automatically adapt these working parameters.

When an l_1 -ball projection has a closed form, its gradient would have a closed form as well. For example, for the vector-norm l_1 -ball projection with $\theta_i = \text{sign}(\beta_i)(|\beta_i| - \tilde{\mu})_+$, the gradient is $\partial \theta_i / \partial \beta_i = (1 - 1/c) \mathbb{I}(|\beta_i| > \tilde{\mu})$, $\partial \theta_i / \partial \beta_j = (-1/c) \mathbb{I}(|\beta_i| > \tilde{\mu}) \mathbb{I}(|\beta_j| > \tilde{\mu})$ for $i \neq j$. In practice, the gradient calculation is conducted via the auto-differentiation framework. Many other l_1 -ball projections have closed forms, including those for rank selection or group sparsity; Chapter 6 of Beck (2017) contains many useful examples.

On the other hand, when the projection lacks a closed form and requires an iterative algorithm for its calculation, we need to numerically evaluate its gradient. When β is in a low-dimensional space, we use finite difference approximation for the j -th entry: $\partial P_{\mathbb{B}_{h,r}}(\beta) / \partial \beta_j \approx$

Table 1: Comparing running time and effective sample size.

(n, p, c_0)	l_1 -ball-HMC	SS-Gibbs	(n, p, c_0)	l_1 -ball-HMC	SS-Gibbs
(200, 500, 25)	216.92	183.30	(200, 500, 25)	11.30%	2.45%
(500, 1000, 50)	238.82	2621.69	(500, 1000, 50)	3.68%	0.8%

(a) Running time (in seconds) for 1,000 iterations (b) Effective sample size of $|C|$ in the Markov of Markov Chain. SS-Gibbs runs very slowly when chains. p is large.

$[P_{\mathbb{B}_{h,r}}(\beta + \varepsilon e_j) - P_{\mathbb{B}_{h,r}}(\beta)]/\varepsilon$, where e_j is the j -th standard basis and $\varepsilon > 0$. When β is in a high-dimensional space, to avoid the high cost of evaluating the projection for $(p + 1)$ times, we use the simultaneous perturbation stochastic approximation (Spall, 1992), which reduces the times of projection evaluation to $(m + 1)$:

$$\frac{\partial P_{\mathbb{B}_{h,r}}(\beta)}{\partial \beta_j} \approx \frac{1}{m} \sum_{k=1}^m [P_{\mathbb{B}_{h,r}}(\beta + \varepsilon \Delta^{(k)}) - P_{\mathbb{B}_{h,r}}(\beta)] / (\varepsilon \Delta_j^{(k)}),$$

where $\Delta^{(k)} = \{\Delta_1^{(k)}, \dots, \Delta_p^{(k)}\}$ has each $\Delta_j^{(k)} \in \{-1, 1\}$ independently generated from Rademacher distribution. It is worth clarifying that, even when an approximate gradient is used, the HMC algorithm satisfies the detailed balance condition thanks to the Metropolis-Hastings adjustment. Therefore, the accuracy of the approximate gradient would only impact the acceptance rate and not the invariant distribution of the Markov chains. Empirically, we find that $m = 20$ and $\varepsilon = 10^{-5}$ achieve good acceptance rate.

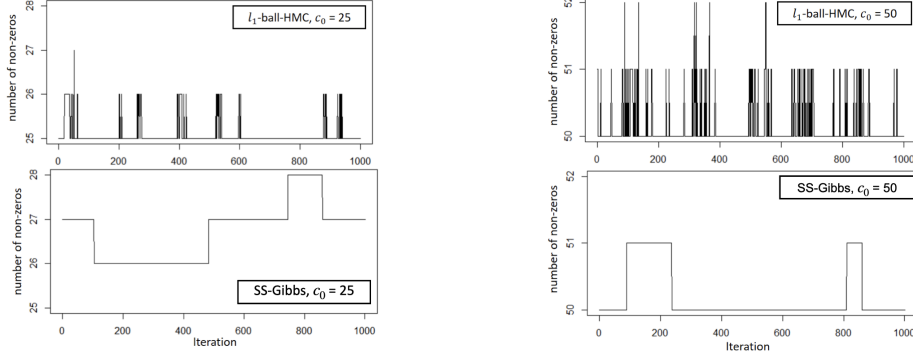
C Benchmark of Algorithms on Sampling from Spike-and-Slab Posterior

As the spike-and-slab prior can be written as a special case of l_1 -ball prior, we compare the computational efficiency using the Hamiltonian Monte Carlo (henceforth named the l_1 -ball-HMC) with the one using the Gibbs sampling algorithm [henceforth named the SS-Gibbs]. The latter is implemented as a Gibbs sampler that draws each variable inclusion indicator given the parameters and then draws the parameter given the indicators.

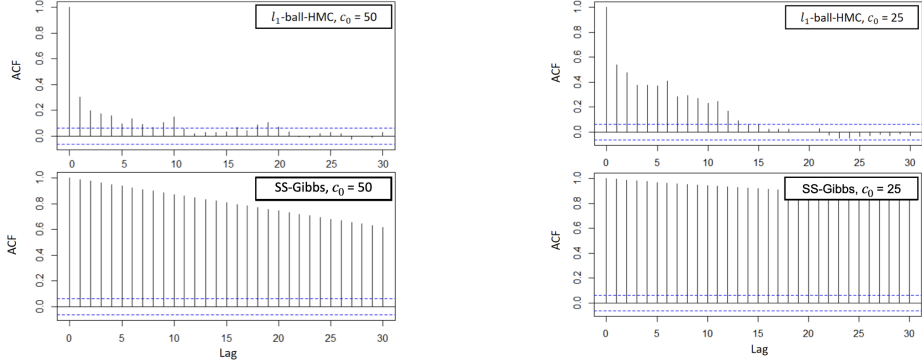
To clarify, for a linear model under a normal likelihood and conjugate priors for coefficients θ and variance σ^2 , one could integrate out the values of θ and σ^2 , and obtain a marginal posterior on $b_i = \mathbb{I}(\theta_i \neq 0)$ for $i = 1, \dots, p$. This leads to the stochastic search variable selection algorithm (George and McCulloch, 1995), which enjoys excellent mixing performance. On the other hand, since in this article we compare with the general class of spike-and-slab priors that (i) may not necessarily lead to posterior conjugacy, and (ii) may be used in non-linear models, we use the Gibbs sampler that updates all parameters (θ, σ^2) without any marginalization.

We use linear models $y \sim N(X\theta^0, \sigma^2 I_n)$ with different (n, p) and let the number of non-zeros c_0 to be $0.05p$. The entries in X are iid standard normal. We let the non-zero entries be 1 and set $\sigma = 0.1$. We compare running time per thousand iterations and examine the mixing performance (the ability of each Markov Chain to explore alternative high-probability models and the effective sample size) in each setting. As shown in Table 1 (a), SS-Gibbs requires much longer running time at $n = 500$ and $p = 1000$. The combinatorial search in the variable indicator causes heavy burden in computation (2622 seconds for 1000 iterations). Meanwhile, the l_1 -ball-HMC is less affected by the increase in dimension.

On the mixing performance, Figure 7 shows that l_1 -ball-HMC can quickly transition between states with different numbers of non-zeros $|C|$, whereas SS-Gibbs suffers from slow mixing with only a few changes in 1,000 iterations. This is reflected in 1(b) as the effective sample size from l_1 -ball-HMC is almost an order higher than the one from SS-Gibbs.



(a) Traceplot of number of nonzeros ($|C|$) in the posterior when $c_0 = 25$. (b) Traceplot of number of nonzeros ($|C|$) in the posterior when $c_0 = 50$.



(c) ACF plot of $|C|$ in the posterior when $c_0 = 25$. (d) ACF plot of $|C|$ in the posterior when $c_0 = 50$.

Figure 7: Comparing mixing performance of the l_1 -ball-HMC (upper rows) with the SS-Gibbs (lower rows) in $n = 200, p = 500, c_0 = 25$ and $n = 500, p = 1000, c_0 = 50$. Under both settings, the l_1 -ball-HMC enjoys faster mixing with rapid changes between different numbers of non-zeros $|C|$, while SS-Gibbs tends to be stuck at the same $|C|$ for a long time.

D Benchmark in Linear Regression

As discussed in the theory section, in the linear regression, the recovery of θ^0 requires some conditions on the cardinality of the true parameter c_0 , and the sample size n . We now use numerical simulations to empirically estimate the sparsity detection limits and the required minimum sample size.

For each experiment setting, the n rows of the design matrix $X \in \mathbb{R}^{n \times p}$ are independently drawn from $N(0, I_p)$. We generate the true θ^0 according to the level of sparsity, where the non-zero entries are drawn from $N(5, 1^2)$. We experiment with $p = 200, 300, 500$ and 800 , with n being a multiple of p and c_0 set to 25, 50, 75, 100, 150, 200 times $\sqrt{1/\log p}$, as corresponding to

different degrees of sparsity. To be consistent with the theory result on regression, we benchmark the sup-norm $\sup_i \|\hat{\theta}_i - \theta_i^0\|$ between the posterior mean $\hat{\theta}$ and the oracle θ^0 . We plot the results in Figure 8, and make a few observations: (i) when $n \geq p$, all settings have low estimation errors close to zero; (ii) when $n < p$, we have good result roughly when $c_0 \leq 2\sqrt{n/\log p}$. This range is coherent with our theoretic analysis.

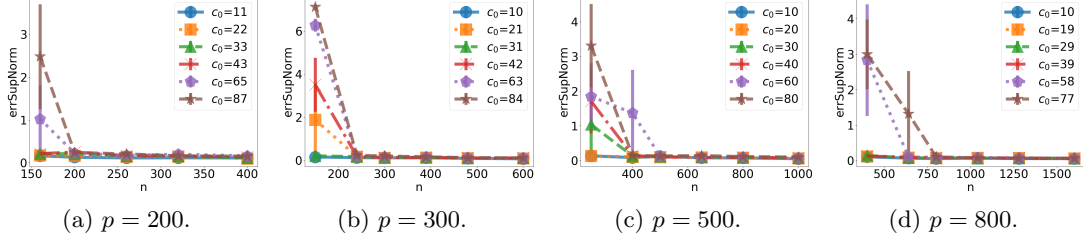


Figure 8: The simulation in sparse regression shows the l_1 -ball prior can correctly recover θ^0 in l_∞ norm when $c_0 \lesssim 2\sqrt{n/\log p}$.

Next, we compare the performance of the l_1 -ball prior with the Bayesian lasso and horseshoe priors, over a range of different p , n and c_0 . We benchmark using the canonical normal means (hence $n = p$) problem $y_i = \theta_i + \epsilon_i$ for $i = 1, \dots, n$, and $\epsilon_i \stackrel{\text{iid}}{\sim} N(0, 1^2)$, and compare with two Bayesian continuous priors: the horseshoe (Carvalho et al., 2010) and the Bayesian lasso (Park and Casella, 2008), implemented through R packages `horseshoe` and `monomvn`. The true non-zero entries in θ are drawn from $N(10, 1^2)$. We consider $n = 200$ and 500. For each n , we let the true cardinality be $c_0 = 5, 10$ and 20. For the l_1 -ball prior, we choose $\beta_i \sim \text{DE}(0, \lambda_i \sigma)$ with scale $\lambda_i \stackrel{\text{iid}}{\sim} \text{Exp}(1)$, and $r \sim \text{Exp}(10)$. For the Bayesian Lasso, we choose prior $\theta_i \stackrel{\text{iid}}{\sim} \text{DE}(0, 0.5\sigma)$. For the horseshoe prior, we use the default scaled half-Cauchy $C^+(0, \sigma)$ prior for the global scale τ . For all three methods, we use the Jeffreys prior for σ^2 , $\pi_{\sigma^2}(\sigma^2) \propto \sigma^{-2}$. We run 10,000 MCMC steps for each model, and discard the first 5,000 steps as burn-in.

We use the posterior mean $\hat{\theta}$ to compute the mean squared error, $\|\hat{\theta} - \theta^0\|_2^2$. We also compute the estimated cardinality \hat{c} based on $\hat{\theta}$. Since the continuous shrinkage priors do not produce exact zero, we adopt the strategy in Carvalho et al. (2010), the i -th entry is viewed as non-zero if $|\hat{\theta}_i/y_i| > 0.5$.

As shown in Figure 9, Panel (a) and (b), the l_1 -ball and the horseshoe methods are comparable in parameter estimation, with smaller errors than the Bayesian lasso. Panel (c) and (d) show that the l_1 -ball method gives a satisfactory estimation of the cardinality, and the horseshoe produces similarly good results although with a slight over-estimation (which could be reduced with some further tuning on its global scale parameter).

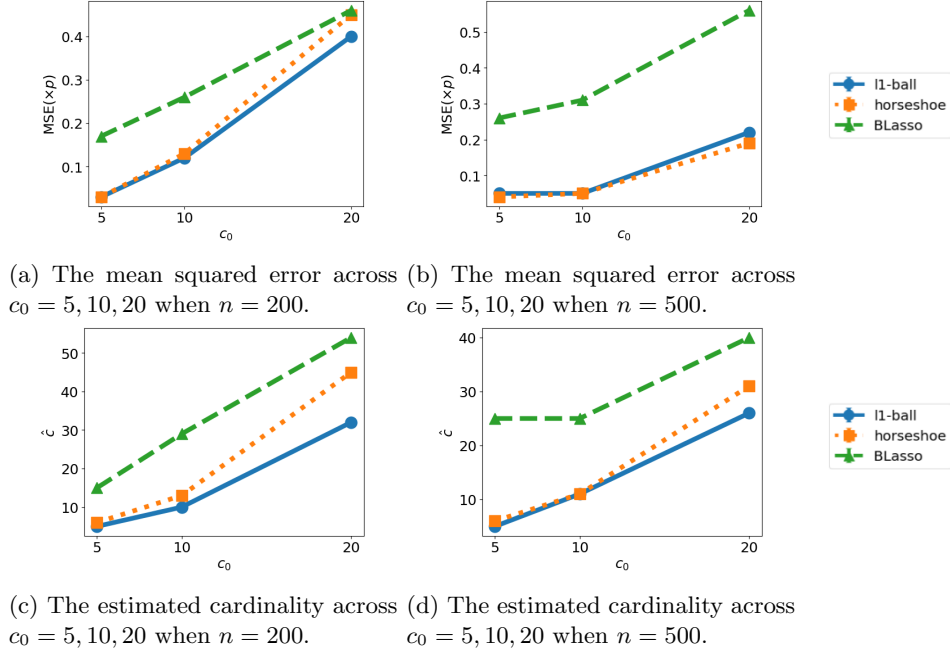


Figure 9: Comparing the l_1 -ball, the horseshoe and the Bayesian lasso in different dimensionality and sparsity levels. The l_1 -ball method gives a satisfactory estimation of the cardinality.

E Comparison with Post-processing Methods

E.1 Methodological Comparison with Post-processing Methods

There have been some works that post-process the posterior samples when modeling under continuous priors. Bondell and Reich (2012) use a conjugate continuous prior for θ (without imposing any shrinkage apriori) to first estimate high posterior density region associated with $(1 - \alpha)$ probability, within which they extract a sub-region by minimizing the $\|\theta\|_0$ (l_0 -norm of θ). Similarly, Hahn and Carvalho (2015) use a shrinkage prior for θ and estimate the posterior mean and variance of θ , then find a summary point estimate $\hat{\theta}$ that minimizes a loss function consisting of squared prediction error and l_0 -norm. Li and Pati (2017) use a shrinkage prior for θ , then use 2-means to cluster each posterior sample into two groups, with the goal of finding a point estimate on the number of non-zero θ_j 's as represented by the size of one cluster.

In the scope of variable selection in regression, those post-processing approaches produce a point estimate $\hat{\theta}$ (Hahn and Carvalho, 2015; Li and Pati, 2017), or a set of sparse θ associated with zero posterior probability (Bondell and Reich, 2012). In a diagram, those estimates are produced from two stages,

$$(i) \theta \sim \frac{\mathcal{L}(y; \theta) \pi_{\theta}(\theta)}{\int \mathcal{L}(y; \theta) \pi_{\theta}(\theta) d\theta}, \quad (ii) \theta^* = T(\theta),$$

for some transformation T . While being well motivated for other purposes (such as ease of interpretation), the key issue is in the lack of a tractable probabilistic characterization on the transform T . As a result, these approaches cannot be used for uncertainty quantification, such

Table 2: False positive rate and false negative rate under independent design matrix.

$(n, p, c_0, \theta_{C_0})$	l_1 -ball	S2M	PCR
(50, 300, 10, 5)	(0.0, 0.0)	(0.020, 0.60)	(0.021, 0.80)
(50, 300, 10, 10)	(0.0, 0.0)	(0.013, 0.30)	(0.020, 0.60)
(50, 300, 30, 10)	(0.085, 0.77)	(0.081, 0.73)	(0.104, 0.93)
(200, 1000, 10, 5)	(0.0, 0.0)	(0.0, 0.0)	(0.01, 0.10)
(200, 1000, 10, 10)	(0.0, 0.0)	(0.0, 0.0)	(0.003, 0.30)
(200, 1000, 50, 10)	(0.017, 0.34)	(0.025, 0.48)	(0.043, 0.82)

as estimating the $(1 - \alpha)$ -credit interval on $\|\theta\|_0$ and $(1 - \alpha)$ -prediction interval for $x^{*T}\theta$ for a new x^* .

On the other hand, our proposed l_1 -ball and generalized l_1 -ball priors are fully Bayesian. The projection $\theta = P_{\mathbb{B}}(\beta)$ induces a proper combinatorial prior with positive probability in either θ or some transformation of θ . With a likelihood function of θ , one could estimate the canonical posterior distribution $\Pi(\theta | y)$ and conduct uncertainty quantification via standard Bayesian procedures. The key idea is using l_1 -ball projection $\theta = P_{\mathbb{B}}(\beta)$ as a many-to-one mapping, to *reparameterize* θ . Similarly, in a diagram, our modeling framework is

$$\theta \sim \frac{\mathcal{L}(y; \theta) \pi_{\theta}(\theta)}{\int \mathcal{L}(y; \theta) \pi_{\theta}(\theta) d\theta}, \quad \text{where } \theta = P_{\mathbb{B}}(\beta).$$

In the above, optimization algorithms serve as means to compute such a reparameterization, and are only required when $P_{\mathbb{B}_{h,r}}(\beta)$ do not have closed-form solution (in the generalized l_1 cases).

E.2 Numerical Comparison on Point Estimates

Besides the difference in the capability of uncertainty quantification, we further show performance differences in the accuracy of point estimates.

We extract zero/non-zero labels from Fréchet mean generated by the l_1 -ball and point estimates generated by the joint set penalized credible regions method (PCR) (Bondell and Reich, 2012) and the sequential 2-Means clustering (S2M) method (Li and Pati, 2017). We then compare their false positive rates and false negative rates.

The data are generated from $y \sim N(X\theta^0, \sigma^2 I)$. We fix $\sigma = 1$, and experiment with different settings of n, p, c_0 and signal strength in the non-zeros (θ_{C_0}). We test with both independent design matrix $X_{i,j} \stackrel{\text{iid}}{\sim} N(0, 1^2)$ and correlated design matrix with each row of X from $N(0, I)$ or $N(0, \Sigma)$, $\Sigma_{j,k} = 0.5^{|j-k|}$. For the PCR, we obtain 5,000 MCMC samples from the conjugate Gaussian prior and use the joint credible set results. For the S2M, we first obtain 5,000 MCMC samples under a horseshoe prior (Carvalho et al., 2010), then apply the sequential 2-means algorithm. The comparison results are listed in Table 2 and 3. The three methods are comparably good with large sample size, but the l_1 -ball prior method outperforms the post-processing methods in small (n, p) cases.

Table 3: False positive rate and false negative rate under correlated design matrix.

$(n, p, c_0, \theta_{C_0})$	l_1 -ball	S2M	PCR
(50, 300, 10, 5)	(0.0, 0.0)	(0.0, 0.0)	(0.010, 0.30)
(50, 300, 10, 10)	(0.0, 0.0)	(0.0, 0.0)	(0.006, 0.20)
(50, 300, 30, 10)	(0.037, 0.33)	(0.044, 0.40)	(0.070, 0.63)
(200, 1000, 10, 5)	(0.0, 0.0)	(0.0, 0.0)	(0.0, 0.0)
(200, 1000, 10, 10)	(0.0, 0.0)	(0.0, 0.0)	(0.0, 0.0)
(200, 1000, 50, 10)	(0.001, 0.02)	(0.001, 0.02)	(0.013, 0.26)

F Change Point Detection

To show that the exact zeros are essential for the success of the l_1 -tricks, we first experiment with a change point detection model and compare the results with the continuous shrinkage prior.

We use the simulated data with $y_t \mid \mu_t \sim N(\mu_t, \sigma^2)$ for $t = 1, \dots, 100$, where μ_t is piecewise constant from $\{30, 10, 40, 20\}$ with three change points at $t \in \{20, 40, 80\}$. In order to compare with the continuous shrinkage prior, we re-parameterize this as a linear regression problem using $\theta_t = \mu_t - \mu_{t-1}$:

$$y_t = \sum_{i=1}^t \theta_i + \epsilon_t, \quad \epsilon_t \sim N(0, \sigma^2), \quad t = 1, \dots, 100,$$

where we use $\sigma^2 = 10$ during the data generation. This enables us to impose sparsity on θ_t , as the curve is a flat line in $[t, t+d]$ if $\theta_t = \theta_{t+1} = \dots = \theta_{t+d} = 0$, and nonzero values only occur at the sudden changes. We use the l_1 -ball prior on θ_i ; to compare, we also test the model with a horseshoe prior on θ_i (Carvalho et al., 2010). In both cases, we use the Jeffreys prior $\pi_{\sigma^2}(\sigma^2) \propto 1/\sigma^2$.

As shown in Figure 10 (c), under the l_1 -ball prior, we obtain the posterior curves in step functions, as desired in this model. On the other hand, the horseshoe prior could not produce a step function, due to the small increments/decrements accumulating over time (e), leading to a clear departure from a step function curve.

To be fair, this is an expected result as the continuous shrinkage prior is not designed for handling such a problem. In fact, comparing Panels b and d, the horseshoe prior here has a good performance in the uncertainty quantification on each of θ_i . However, a key difference is in the *joint* probability of all θ_i 's — in this case, the horseshoe prior does not have a large probability for the neighboring θ_i 's to have $\sum_{i=t}^{t+d} |\theta_i| = 0$; whereas the l_1 -ball does have this property, since all these small β_i 's with $|\beta_i| \leq \tilde{\mu}$ are now reduced to exactly zero.

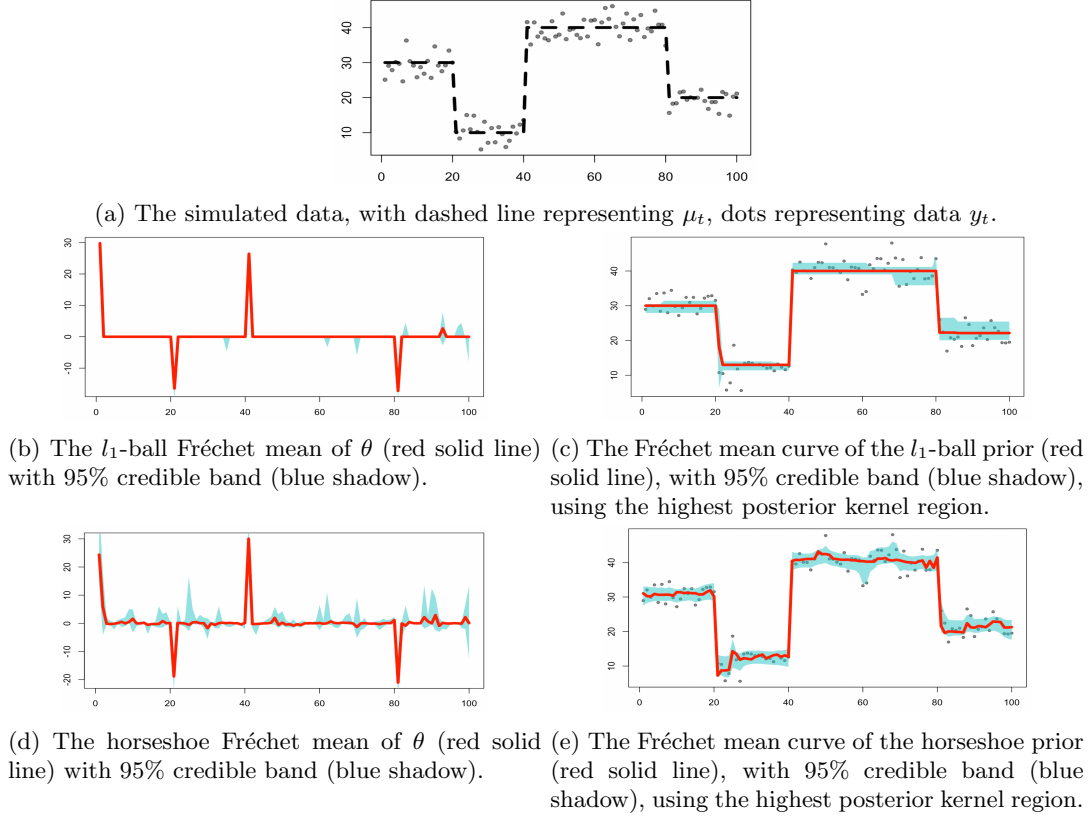


Figure 10: Comparing the performances of applying l_1 -ball prior and continuous shrinkage prior in the change point detection model: the l_1 -ball produces a step function with a few steps corresponding to the major changes, whereas the continuous shrinkage prior produces small increments/decrements that accumulate over time to a non-trivial departure from a step function.

G Additional Experiments

G.1 Structured Sparsity: Inducing Dependency among Zeros

We want to show how the l_1 -ball prior can easily incorporate structured sparsity assumption (Hoff, 2017; Griffin and Hoff, 2019), where those zeros may have an inherent dependency structure.

To give more specifics, we present an application of improving network estimation on human brain functional connectivity, using prior information from the structural connectivity. The raw data of the former are an affinity matrix with scores $A_{i,j} \in [-1, 1]$ between 1,000 voxels collected from a functional magnetic resonance imaging (fMRI) on tracking their blood oxygen levels, and the latter is from a diffusion tensor imaging (DTI) that measures the white matter tractography in terms of observed probability $S_{i,j} \in [0, 1]$ that two voxels are anatomically connected (with $S_{i,i} = 0$ on the diagonal) (Cole et al., 2021).

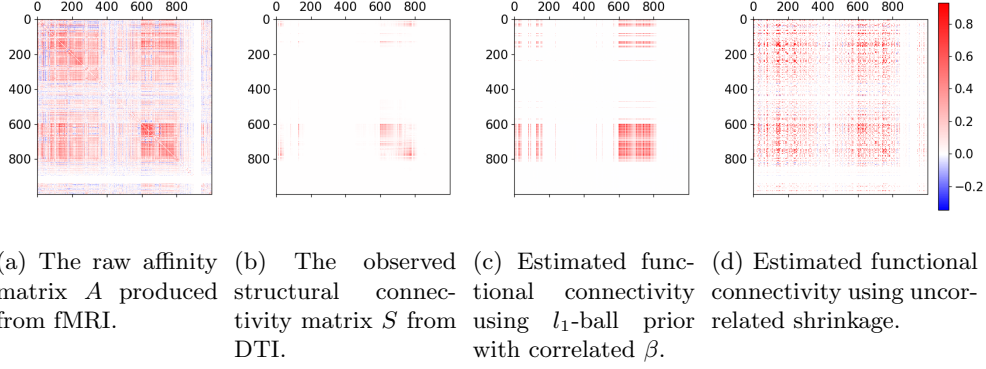


Figure 11: Improving low-rank functional connectivity estimates [from (a) to (c)] by inducing dependency among the zeros under an l_1 -ball prior. The dependency comes from a correlation structure on β according to the structural connectivity (b), and project to θ . In comparison, uncorrelated shrinkage (d) does not enjoy such a structured sparsity, as it tends to pick up the large values from (a). Fréchet means are shown in (c) and (d).

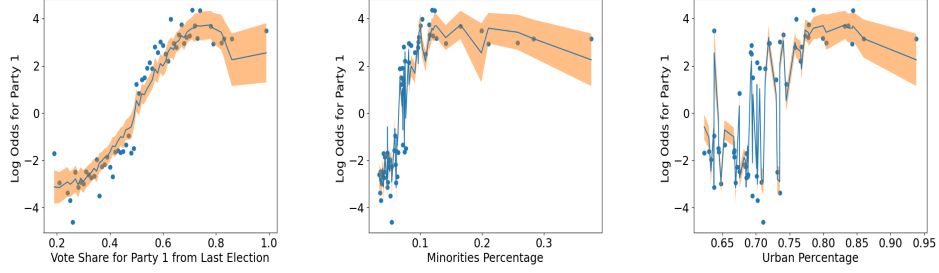
Due to that the affinity scores in A are calculated based on some heuristic post-processing of the multivariate time series data from fMRI, there are often a large number of spurious associations. Therefore, it is useful to borrow information from the structural connectivity to model functional connectivity (Honey et al., 2009; Bassett et al., 2018; Zhu et al., 2014). That is, when the structural connectivity is small $S_{i,j} \approx 0$, then the chance of finding a functional connectivity should be small (whereas an $S_{i,j} \approx 1$ does not necessarily mean a high functional connectivity). Following common low dimensional modeling strategy (Hoff et al., 2002) for a network, we use

$$\begin{aligned}
 A &= \sum_{k=1}^d \lambda_k \theta_k \theta_k^T + \mathcal{E}, \quad \mathcal{E}_{i,j} \stackrel{\text{iid}}{\sim} N(0, \sigma^2), \quad \mathcal{E}_{j,i} = \mathcal{E}_{i,j} \text{ for } i < j, \\
 \theta_k &= P_{\mathbb{B}_r}(\beta_k), \quad \beta_k \sim N(0, J - S + \kappa I), \\
 \lambda &= P_{\mathbb{B}_r}(\gamma), \quad \gamma_k \stackrel{\text{iid}}{\sim} \text{Exp}(1) \quad \text{for } k = 1, \dots, d.
 \end{aligned} \tag{18}$$

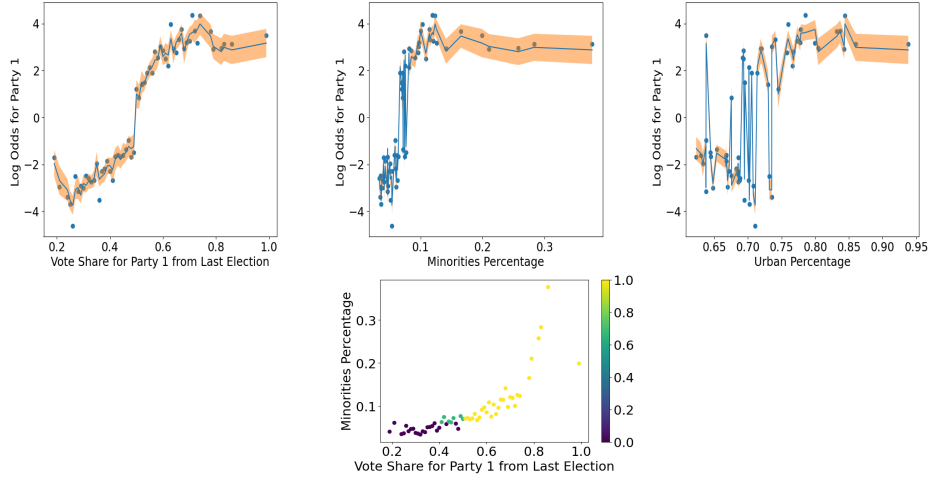
where J is a matrix of ones, and $\kappa \geq 0$ is a constant to make the covariance positive definite; for our S , we use $\kappa = 0$. We use $d = 10$ and an l_1 -ball prior to induce some $\lambda_k = 0$ [in the Fréchet mean, we have effectively 2 non-zero λ_k 's]. In the above model, when $S_{i,j} \approx 0$, we would have $\beta_{k,i}$ and $\beta_{k,j}$ strongly correlated for $k = 1, \dots, d$, hence $\theta_{k,i}$ and $\theta_{k,j}$ have a large chance to be simultaneously zero a priori; on the other hand, when $S_{i,j} \approx 1$, $\theta_{k,i}$ and $\theta_{k,j}$ are less correlated, hence $S_{i,j}$ has less influence on the estimate.

Figure 11 shows how this model borrows information from structural connectivity (panel b) to make a sparse estimate on the functional connectivity (panel c). Compared to the raw affinity matrix (panel a), the majority of the functional connectivity among the first 400 voxels are shrunk to zero, since there is little structural connectivity. To compare, we apply the same model except with $\beta_k \sim N(0, I)$ and plot the estimate (in panel d); without imposing dependency among those zeros, the estimated matrix is close to picking up the large affinity scores from A .

G.2 Additional Results of Discontinuous Gaussian Process Regression



Fitting a continuous Gaussian process with squared exponential covariance.



Fitting a discontinuous Gaussian process with latent jittering coordinates (with the values of η_i shown in the last panel).

Figure 12: Discontinuous Gaussian process regression on the election data. With a latent jittering coordinate η_i regularized by a generalized l_1 -ball prior, we can change a Gaussian process with squared exponential covariance function (first row) to have discontinuities, giving an improved fit to the data (second row). The fitted curves and 95% point-wise credible bands are shown.

Figure 12 compares the fitting continuous and discontinuous Gaussian process regression models to the election data, using all three predictors. The root-mean-square deviation (RMSD) is 0.315 for the discontinuous model, and is 0.427 for the continuous one. The discontinuous Gaussian process finds three distinct values in η_i 's.

G.3 Additional Results of the Sparse Change Detection Data Application

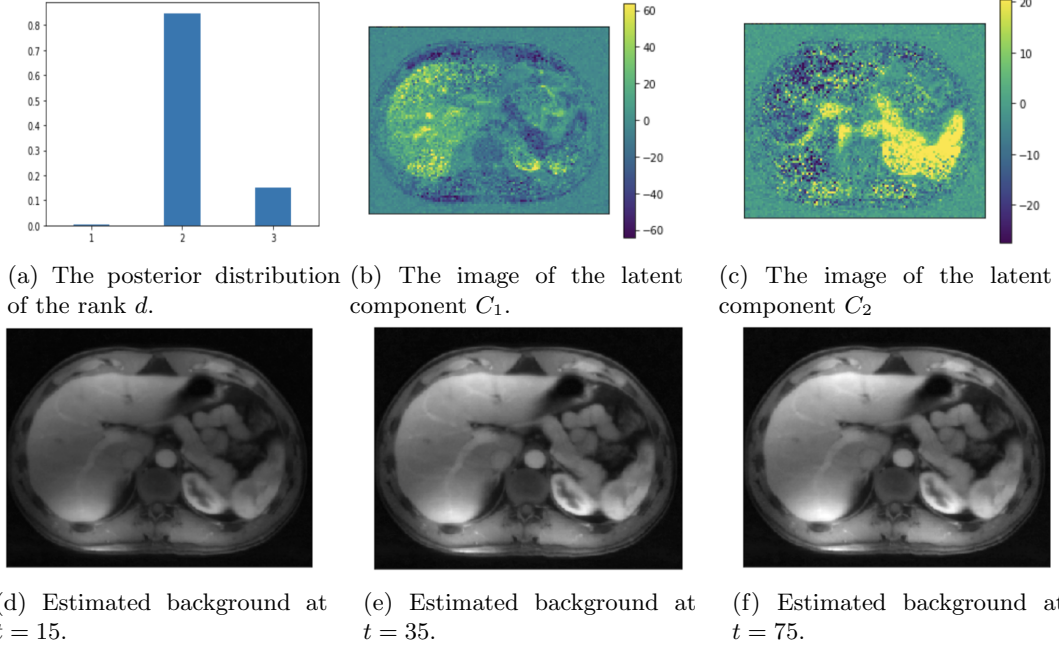


Figure 13: The low-rank modeling of the video background L , where L is a flattened matrix containing all the background images over 75 time points. The posterior distribution is concentrated at a low rank $d = 2$ for the matrix L (panel a). This captures the subtle changes that happen in the background, such as the brightness between (d) and (f).

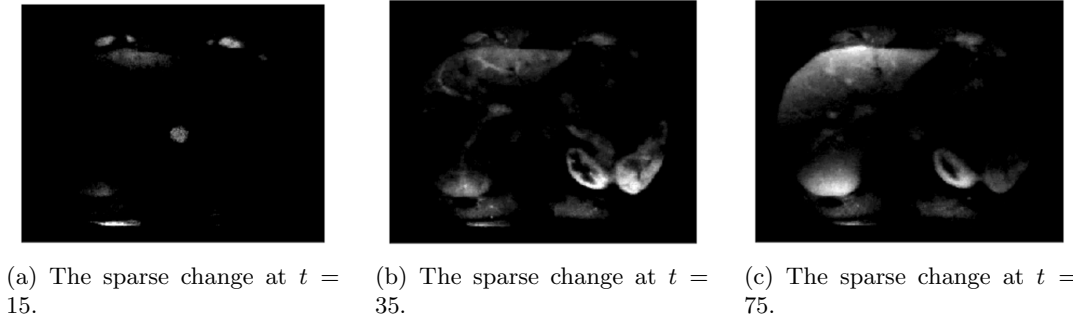


Figure 14: The sparse change S_t with a time-invariant background. Compared to Figure 5 in the article, these sparse estimates fail to reveal details under the slowly changing background: (a) does not highlight the aorta enhancement; (b) and (c) involve too much light change, so that the detailed liver and portal vein enhancement are blurred.

G.4 Simulation on Rank Estimation

We now use a simulation to empirically illustrate the performance of rank estimation with the generalized l_1 -ball prior using the nuclear norm. We first generate a set of p -element vectors

ϕ_1, \dots, ϕ_d with $\phi_{k,i} \stackrel{\text{iid}}{\sim} N(0, 5^2)$, and a set of T -element vectors $\tilde{\alpha}_1, \dots, \tilde{\alpha}_d$ with $\tilde{\alpha}_{k,i} \stackrel{\text{iid}}{\sim} N(0, 1^2)$. Then we obtain a $p \times T$ matrix $M = \sum_{k=1}^d \phi_k (\tilde{\alpha}_k)^T + \mathcal{E}$, where each entry in the noise matrix \mathcal{E} is generated from iid $N(0, 1^2)$. We model the simulated data by

$$M = L + \mathcal{E},$$

$$L = \underset{Z \in \mathbb{R}^{p \times T}, \|Z\|_* \leq r}{\operatorname{argmin}} \|Z - \beta\|_F^2, \quad \beta_{ij} \stackrel{\text{iid}}{\sim} N(0, \sigma_\beta^2).$$

where we set $\sigma_\beta^2 = 5^2$, $r \sim \text{Exp}(10)$. Figure 15 shows the posterior distribution of the rank in the $(d, T) = (5, 25)$ and $(10, 50)$ settings, with $p = 25$. In both cases, the nuclear-norm based l_1 -ball prior successfully recovers the true rank.

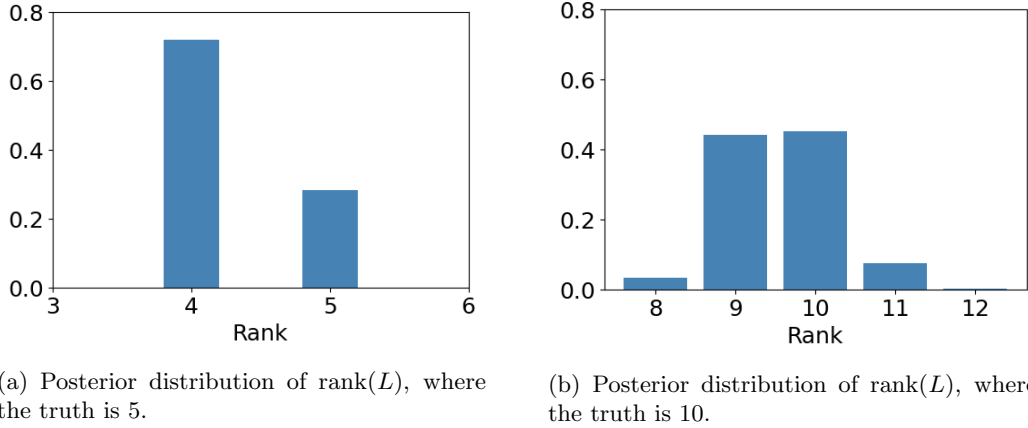


Figure 15: Simulation for the rank estimation using the nuclear-norm l_1 -ball prior.

References

- Anderson Jr, W. N. and T. D. Morley (1985). Eigenvalues of the Laplacian of a Graph. *Linear and Multilinear Algebra* 18(2), 141–145.
- Armagan, A., D. B. Dunson, and J. Lee (2013). Generalized Double Pareto Shrinkage. *Statistica Sinica* 23(1), 119.
- Bai, R. and M. Ghosh (2019). On the Beta Prime Prior for Scale Parameters in High-Dimensional Bayesian Regression Models. *Statistica Sinica*.
- Banerjee, S. and S. Ghosal (2013). Bayesian Estimation of a Sparse Precision Matrix. *arXiv preprint arXiv:1309.1754*.
- Bassett, D. S., P. Zurn, and J. I. Gold (2018). On the Nature and Use of Models in Network Neuroscience. *Nature Reviews Neuroscience* 19(9), 566–578.
- Beck, A. (2017). *First-order Methods in Optimization*. SIAM.
- Bhattacharya, A., A. Chakraborty, and B. K. Mallick (2016). Fast Sampling With Gaussian Scale Mixture Priors in High-Dimensional Regression. *Biometrika*, asw042.

- Bhattacharya, A. and D. B. Dunson (2011). Sparse Bayesian Infinite Factor Models. *Biometrika*, 291–306.
- Bhattacharya, A., D. Pati, N. S. Pillai, and D. B. Dunson (2015). Dirichlet–Laplace Priors for Optimal Shrinkage. *Journal of the American Statistical Association* 110(512), 1479–1490.
- Bondell, H. D. and B. J. Reich (2012). Consistent High-dimensional Bayesian Variable Selection via Penalized Credible Regions. *Journal of the American Statistical Association* 107(500), 1610–1624.
- Boyd, S., N. Parikh, and E. Chu (2011). *Distributed Optimization and Statistical Learning via the Alternating Direction Method of Multipliers*. Now Publishers Inc.
- Breth, M. (1978). Bayesian Confidence Bands for a Distribution Function. *The Annals of Statistics* 6(3), 649–657.
- Bühlmann, P. and S. Van De Geer (2011). *Statistics for High-dimensional Data: Methods, Theory and Applications*. Springer Science & Business Media.
- Carvalho, C. M., N. G. Polson, and J. G. Scott (2010). The Horseshoe Estimator for Sparse Signals. *Biometrika* 97(2), 465–480.
- Castillo, I., J. Schmidt-Hieber, and A. Van der Vaart (2015). Bayesian Linear Regression with Sparse Priors. *The Annals of Statistics* 43(5), 1986–2018.
- Castillo, I. and A. van der Vaart (2012). Needles and Straw in a Haystack: Posterior Concentration for Possibly Sparse Sequences. *The Annals of Statistics* 40(4), 2069–2101.
- Chen, S. S., D. L. Donoho, and M. A. Saunders (2001). Atomic Decomposition by Basis Pursuit. *SIAM Review* 43(1), 129–159.
- Cole, M., K. Murray, E. St-Onge, B. Risk, J. Zhong, G. Schifitto, M. Descoteaux, and Z. Zhang (2021). Surface-Based Connectivity Integration: An Atlas-free Approach to Jointly Study Functional and Structural Connectivity. *Human Brain Mapping* 42(11), 3481–3499.
- Cuturi, M. (2013). Sinkhorn Distances: Lightspeed Computation of Optimal Transport. *Advances in Neural Information Processing Systems* 26, 2292–2300.
- Duchi, J., S. Shalev-Shwartz, Y. Singer, and T. Chandra (2008). Efficient Projections onto the L_1 -Ball for Learning in High Dimensions. In *Proceedings of the 25th International Conference on Machine Learning*, pp. 272–279.
- Efron, B., T. Hastie, I. Johnstone, and R. Tibshirani (2004). Least Angle Regression. *The Annals of Statistics* 32(2), 407–499.
- Fan, J., H. Liu, Y. Ning, and H. Zou (2017). High Dimensional Semiparametric Latent Graphical Model for Mixed Data. *Journal of the Royal Statistical Society: Series B (Statistical Methodology)* 79(2), 405–421.
- Federer, H. (2014). *Geometric Measure Theory*. Springer.
- George, E. I. and R. E. McCulloch (1995). Stochastic Search Variable Selection. *Markov Chain Monte Carlo in Practice* 68, 203–214.

- Gong, C., C. Han, G. Gan, Z. Deng, Y. Zhou, J. Yi, X. Zheng, C. Xie, and X. Jin (2017). Low-dose Dynamic Myocardial Perfusion CT Image Reconstruction Using Pre-contrast Normal-dose CT Scan Induced Structure Tensor Total Variation Regularization. *Physics in Medicine & Biology* 62(7), 2612.
- Gramacy, R. B. and H. K. H. Lee (2008). Bayesian Treed Gaussian Process Models With an Application to Computer Modeling. *Journal of the American Statistical Association* 103(483), 1119–1130.
- Grave, E., G. R. Obozinski, and F. R. Bach (2011). Trace Lasso: a Trace Norm Regularization for Correlated Designs. In *Advances in Neural Information Processing Systems*, pp. 2187–2195.
- Griffin, M. and P. D. Hoff (2019). Structured Shrinkage Priors. *arXiv preprint arXiv:1902.05106*.
- Gunn, L. H. and D. B. Dunson (2005). A Transformation Approach for Incorporating Monotone or Unimodal Constraints. *Biostatistics* 6(3), 434–449.
- Hahn, P. R. and C. M. Carvalho (2015). Decoupling Shrinkage and Selection in Bayesian Linear Models: a Posterior Summary Perspective. *Journal of the American Statistical Association* 110(509), 435–448.
- Hoff, P. D. (2017). Lasso, Fractional Norm and Structured Sparse Estimation Using a Hadamard Product Parametrization. *Computational Statistics & Data Analysis* 115, 186–198.
- Hoff, P. D., A. E. Raftery, and M. S. Handcock (2002). Latent Space Approaches to Social Network Analysis. *Journal of the American Statistical Association* 97(460), 1090–1098.
- Hoffman, M. D. and A. Gelman (2014). The No-U-Turn Sampler: Adaptively Setting Path Lengths in Hamiltonian Monte Carlo. *Journal of Machine Learning Research* 15(1), 1593–1623.
- Honey, C. J., O. Sporns, L. Cammoun, X. Gigandet, J.-P. Thiran, R. Meuli, and P. Hagmann (2009). Predicting Human Resting-state Functional Connectivity from Structural Connectivity. *Proceedings of the National Academy of Sciences* 106(6), 2035–2040.
- Hu, Y., D. Zhang, J. Ye, X. Li, and X. He (2012). Fast and Accurate Matrix Completion via Truncated Nuclear Norm Regularization. *IEEE Transactions on Pattern Analysis and Machine Intelligence* 35(9), 2117–2130.
- Ishwaran, H. and J. S. Rao (2005). Spike and Slab Variable Selection: Frequentist and Bayesian Strategies. *The Annals of Statistics* 33(2), 730–773.
- Jain, S. and R. M. Neal (2007). Splitting and Merging Components of a Nonconjugate Dirichlet Process Mixture Model. *Bayesian Analysis* 2(3), 445–472.
- Jauch, M., P. D. Hoff, and D. B. Dunson (2020). Monte Carlo Simulation on the Stiefel Manifold via Polar Expansion. *Journal of Computational and Graphical Statistics*, 1–23.
- Jewell, S., P. Fearnhead, and D. Witten (2022). Testing for a Change in Mean After Changepoint Detection. *Journal of the Royal Statistical Society: Series B: Statistical Methodology* in press.
- Lee, D. S., E. Moretti, and M. J. Butler (2004). Do Voters Affect or Elect Policies? Evidence from the US House. *The Quarterly Journal of Economics* 119(3), 807–859.

- Lempers, F. B. (1971). *Posterior Probabilities of Alternative Linear Models*. Rotterdam University Press.
- Li, H. and D. Pati (2017). Variable Selection Using Shrinkage Priors. *Computational Statistics & Data Analysis* 107, 107–119.
- Lin, L. and D. B. Dunson (2014). Bayesian Monotone Regression Using Gaussian Process Projection. *Biometrika* 101(2), 303–317.
- Lindsten, F., H. Ohlsson, and L. Ljung (2011). Clustering Using Sum-of-norms Regularization: with Application to Particle Filter Output Computation. In *2011 IEEE Statistical Signal Processing Workshop (SSP)*, pp. 201–204. IEEE.
- Meinshausen, N. and P. Bühlmann (2006). High-dimensional Graphs and Variable Selection with the Lasso. *The Annals of Statistics* 34(3), 1436–1462.
- Miller, J. W. (2022). Consistency of Mixture Models With a Prior on the Number of Components. *Dependence Modeling (In press)*.
- Miller, J. W. and M. T. Harrison (2014). Inconsistency of Pitman-Yor Process Mixtures for the Number of Components. *Journal of Machine Learning Research* 15(1), 3333–3370.
- Miller, J. W. and M. T. Harrison (2018). Mixture Models with a Prior on the Number of Components. *Journal of the American Statistical Association* 113(521), 340–356.
- Mitchell, T. J. and J. J. Beauchamp (1988). Bayesian Variable Selection in Linear Regression. *Journal of the American Statistical Association* 83(404), 1023–1032.
- Neal, R. M. (2011). MCMC using Hamiltonian Dynamics. In S. Brooks, A. Gelman, G. Jones, and X.-L. Meng (Eds.), *Handbook of Markov Chain Monte Carlo*, Chapter 5. CRC Press.
- Nishimura, A., D. B. Dunson, and J. Lu (2020). Discontinuous Hamiltonian Monte Carlo for Discrete Parameters and Discontinuous Likelihoods. *Biometrika* 107(2), 365–380.
- Otazo, R., E. Candes, and D. K. Sodickson (2015). Low-Rank Plus Sparse Matrix Decomposition for Accelerated Dynamic MRI with Separation of Background and Dynamic Components. *Magnetic Resonance in Medicine* 73(3), 1125–1136.
- Pakman, A. and L. Paninski (2013). Auxiliary-variable Exact Hamiltonian Monte Carlo Samplers for Binary Distributions. *arXiv preprint arXiv:1311.2166*.
- Park, T. and G. Casella (2008). The Bayesian Lasso. *Journal of the American Statistical Association* 103(482), 681–686.
- Polson, N. G. and J. G. Scott (2016). Mixtures, Envelopes and Hierarchical Duality. *Journal of the Royal Statistical Society: Series B: Statistical Methodology*, 701–727.
- Ročková, V. and E. I. George (2018). The Spike-and-slab Lasso. *Journal of the American Statistical Association* 113(521), 431–444.
- Sen, D., S. Patra, and D. Dunson (2018). Constrained Inference Through Posterior Projections. *arXiv preprint arXiv:1812.05741*.
- Shojaie, A. and G. Michailidis (2010). Penalized Likelihood Methods for Estimation of Sparse High-dimensional Directed Acyclic Graphs. *Biometrika* 97(3), 519–538.

- Spall, J. (1992). Multivariate stochastic approximation using a simultaneous perturbation gradient approximation. *IEEE Transactions on Automatic Control* 37(3), 332–341.
- Tan, K. M. and D. Witten (2015). Statistical Properties of Convex Clustering. *Electronic Journal of Statistics* 9(2), 2324.
- Tanner, M. A. and W. H. Wong (1987). The Calculation of Posterior Distributions by Data Augmentation. *Journal of the American Statistical Association* 82(398), 528–540.
- Tibshirani, R. (1996). Regression Shrinkage and Selection via the Lasso. *Journal of the Royal Statistical Society: Series B (Statistical Methodology)* 58(1), 267–288.
- Tibshirani, R., M. Saunders, S. Rosset, J. Zhu, and K. Knight (2005). Sparsity and Smoothness via the Fused Lasso. *Journal of the Royal Statistical Society: Series B (Statistical Methodology)* 67(1), 91–108.
- Tibshirani, R. J. and J. Taylor (2011). The Solution Path of the Generalized Lasso. *The Annals of Statistics* 39(3), 1335–1371.
- Vershynin, R. (2018). *High-dimensional Probability: An Introduction with Applications in Data Science*, Volume 47. Cambridge University Press.
- Xu, S. and Z. Fan (2021). Iterative Alpha Expansion for Estimating Gradient-sparse Signals from Linear Measurements. *Journal of the Royal Statistical Society: Series B (Statistical Methodology)* 83(2), 271–292.
- Yuan, M. and Y. Lin (2006). Model Selection and Estimation in Regression with Grouped Variables. *Journal of the Royal Statistical Society: Series B (Statistical Methodology)* 68(1), 49–67.
- Zhang, T. and H. Zou (2014). Sparse Precision Matrix Estimation via Lasso Penalized D-trace Loss. *Biometrika* 101(1), 103–120.
- Zhu, D., T. Zhang, X. Jiang, X. Hu, H. Chen, N. Yang, J. Lv, J. Han, L. Guo, and T. Liu (2014). Fusing DTI and fMRI Data: a Survey of Methods and Applications. *NeuroImage* 102, 184–191.
- Zou, H. and T. Hastie (2005). Regularization and Variable Selection via the Elastic Net. *Journal of the Royal Statistical Society: Series B (Statistical Methodology)* 67(2), 301–320.
- Zou, H., T. Hastie, and R. Tibshirani (2006). Sparse Principal Component Analysis. *Journal of Computational and Graphical Statistics* 15(2), 265–286.